A QUASI-STEADY MODELING APPROACH OF A HEAT PUMP WATER HEATER SYSTEM WITH EXPERIMENTAL VALIDATION AND ANALYSIS

BY

TEJAS SHAH

THESIS

Submitted in partial fulfillment of the requirements
for the degree of Master of Science in Mechanical Engineering
in the Graduate College of the
University of Illinois at Urbana-Champaign, 2020

Urbana, Illinois

Adviser:

Professor Predrag S. Hrnjak

ABSTRACT

In a heat pump water heater system, the dynamic interdependence between the vapor compression system and the water in the storage tank poses a modeling challenge for steady-state refrigeration system models. The aim of this project is to develop a model and methodology for coupling steady-state vapor compression system modeling with a dynamic condenser cooling medium.

Consequently, a quasi-steady transient model is developed involving a steady-state vapor compression system model in Engineering Equation Solver (EES) and a computational fluid dynamics (CFD) model in ANSYS Fluent for simulating the heat transfer and fluid dynamics in the water tank. The respective models are connected at the interface of the tank wall and the water in the storage tank. The linked modeling process, described in the manuscript, involves iteration between the CFD model of the water tank and the vapor compression system model around a quasi-steady warm up of a heat pump water heating system.

The model is developed around a physical heat pump water heater system. An experimental investigation is also conducted to aid with model validation.

ACKNOWLEDGEMENTS

I first extend my deepest thanks and appreciation to my advisor Professor Pega Hrnjak for granting me this opportunity and for his patience, kindness, and wisdom.

Also, I would like to express my gratitude to Air Conditioning and Refrigeration Center consortium of members for their continued support and generosity in funding projects like this one.

Finally, I would be nowhere without the support and sacrifices of my mom, Darshana, in providing me with the values, the opportunities, and the direction for reaching my full potential.

For my mom and late grandfather

TABLE OF CONTENTS

LIST OF FIGURES

LIST OF TABLES

NOMENCLATURE

ABBREVIATIONS

ACRC	Air Conditioning and Refrigeration Center (research consortium)
COP	coefficient of performance
CFD	computational fluid dynamics
EES	Engineering Equation Solver
HPWH	heat pump water heater
UDF	user defined function
TXV	thermal expansion valve

SYMBOLS

A	area [m^2]
C	heat capacity rate of fluid [W / K]
c_p	specific heat of fluid [J / K kg]
DP	change in pressure [kPa]
ΔT_{lm}	log mean temperature difference [K]
ΔT_{in}	inlet temperature difference between hot / cold media [K]
ϵ	effectiveness of heat exchanger
h	convective heat transfer coefficient [W / m^2 K]
k	thermal conductivity [W / m K]
k_c	thermal contact conductance [W / m^2 K]
L, x	length [m]

$\dot{m}$	mass flow rate [kg / s]
μ	viscosity (bulk fluid) [kg / s m]
NTU	number of transfer units
Nu	Nusselt number
η	overall surface efficiency of a finned surface
P	pressure [kPa]
Pr	Prandtl number
Q”	heat flux [W / m^2]
Q	heat transfer rate [W]
Re	Reynolds number
ρ	density [kg / m^3]
T	temperature [ºC or K]
t	thickness [m]
U	overall heat transfer coefficient [W / m^2 K]
V	velocity [m / s]
z_{cp}	coil pitch [m]

SUBSCRIPTS

r	refrigerant
w	water
ht	horizontal top
hb	horizontal bottom
v	vertical
f	fin

c	contact
xri	expansion valve refrigerant inlet
eri	evaporator refrigerant inlet
en	evaporator nozzle
ero	evaporator refrigerant outlet
eai	evaporator air inlet
cri	condenser refrigerant inlet
cro	condenser refrigerant outlet

CHAPTER 1. INTRODUCTION

1.1 OVERVIEW AND OBJECTIVES

The conventional natural gas water heater is a familiar sight in North American markets given low complexity, low upfront costs, low natural gas prices, and ample space in most homes to locate such a unit. In current times, there are many alternatives. In some cases, this is driven by demand from other parts of the world dealing with a different economic landscapes, lifestyles, and climates. In other cases, this is driven by a desire for lower carbon footprints and a shift towards renewables.

The heat pump water heater (HPWH) is one such alternative. This is a vibrant category itself as various manufacturers have different and sometimes unique and proprietary approaches in how they architect their systems. Additionally, climate and weather at the end use location will also lend to whether the heat pump should source heat from the air or the ground in terms of efficiency and performance.

That being said, the purpose of this project is not to explore the merits of different water heating technologies, but to present a useful modeling approach that can be scaled to apply to different types of systems that have slow but transient (quasi-steady) behavior due to an accumulation of energy on the load

side of a heat exchanger. In the context of a heat pump water heater, rise in tank water temperatures over system operation would be that accumulation of energy.

Figure 1.1: Conventional water heater (left) vs. heat pump water heater (right) under study in this project.

The HPWH unit was meant to be a drop-in replacement for a conventional unit and has coils of refrigerant that wrap around the tank as a means of delivering heat to the water. As the system operates, the increasing temperatures of the water, in turn, affect the properties in the vapor compression system. This dynamic interaction is the motivation for this new modeling approach.

The objectives of this project are to establish an experimental baseline of the physical system and to present and demonstrate a new modeling approach for quasi-steady vapor compression systems.

1.2 Brief Review of Literature

Fardoun et al. (2011) developed a transient quasi-steady model of an air-source HPWH with a water tank external to the vapor compression system. In this case, lumped parameter modeling was utilized, and the modeling of heat transfer in the vapor compression system and water tank are simplified. A similar approach is used by Kim et al. (2003) in which stratification of temperature in the water tank is not considered. A challenge in applying this method of modeling to wrap-around coil condenser HPWHs is the strong interdependence between the vapor compression system and the fluid dynamics and thermal behavior of the water in the storage tank. Furthermore, the heat transfer between each condenser coil and the volume of water local to that coil through the tank wall is governed by the dynamically changing local fluid states and flow characteristics.

CHAPTER 2. SYSTEM DESCRIPTION AND EXPERIMENTAL SETUP

2.1 BACKGROUND

The experimental investigation was conducted on a hybrid-electric HPWH unit manufactured by A.O. Smith for the North American market. The unit is designed to a similar footprint as a conventional water heater, has immersion-type electrical resistance heaters for backup, and features a wrap-around condenser coil that utilizes the water storage as the cooling medium.

During the time of the study, the unit was situated inside an environmental chamber in the ACRC at the Mechanical Engineering Laboratory at the University of Illinois. Slight modifications were made for instrumentation and data-logging capabilities. The experimental facility was designed for long-term operation. For reference, a typical transient warm-up from cold to hot typically takes 5-6 hours.

2.2 ORIGINAL SYSTEM

A schematic of the instrumented R134a vapor compression heat pump system is shown in Figure 2.1. The system is an air-source heat pump with copper coil condenser that wraps around the walls of the stainless-steel water tank of 60-

gallon capacity, and the remainder of the vapor compression system is packaged above of the tank of water.

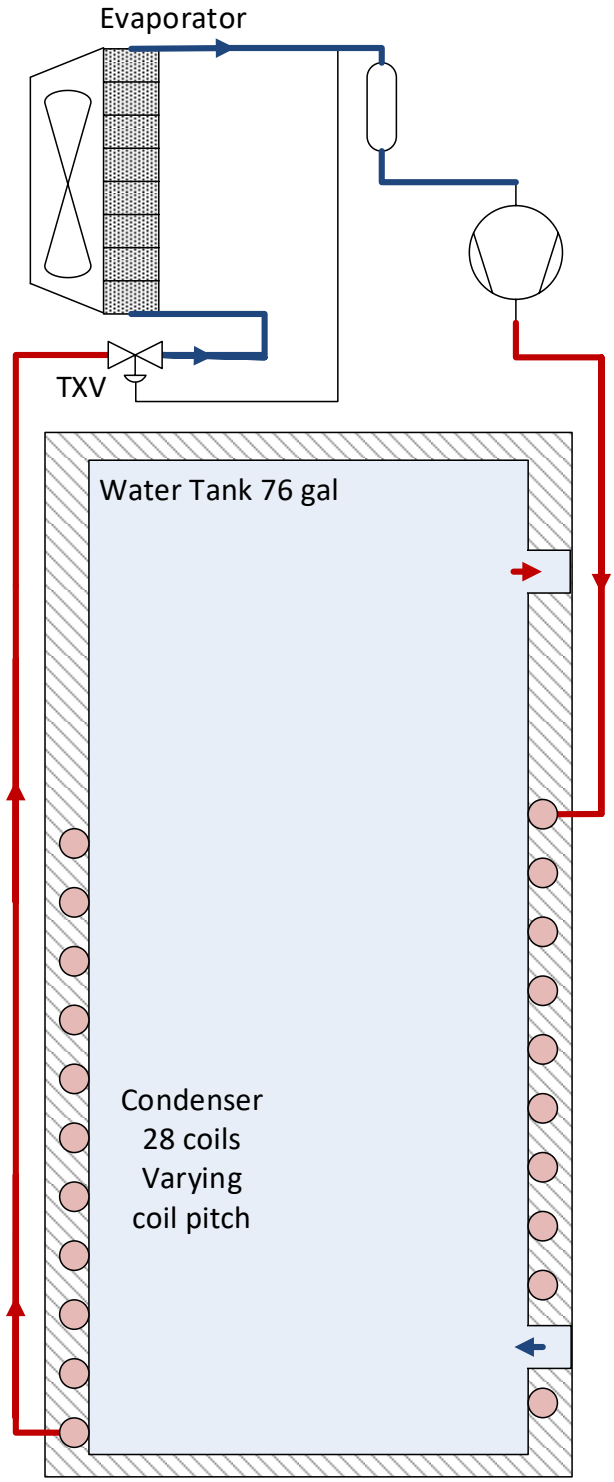

Figure 2.1: Schematic of original system.

As is typical, cold “city-pressure” water enters in the bottom, and hot water would exit at the top, per demand. The system is charged with R134a refrigerant to a nominal of 750g. The evaporator is a 2-circuit fin-and-tube heat exchanger with 13 passes per circuit. The compressor is an Embraco model FCC110HBX. Upstream of the compressor is an accumulator at the outlet of the evaporator.

Not shown in the above schematic are the two electric rod heating elements (one for the upper section of the tank, one for the lower) and an anode (mounted at the top and spanning ~65% of tank height). In a typical end-use application, the electrical heating elements serve as a backup system in times of heavy demand or unfavorable ambient temperatures. In these situations, the heat pump would be too inefficient and unable to meet the heating capacity to serve the hot water demand. An anode protection rod is supplied as in most water heaters to mitigate corrosion inside the tank. These aspects of the system are not relevant to vapor compression system performance or modeling and were thus removed to allow for the necessary instrumentation.

Of specific interest is the coil wrap around the tank. The cross-section of the coil tube is slightly D-shaped to increase the thermal contact patch against the water tank. These coils are spaced with varying pitch from the bottom of the tank to partway up the height of the tank. As the mechanics of heat transfer and fluid flow with respect to this aspect of the design are of particular interest, the coil geometry is presented in Table 2.1.

Table 2.1: Water tank coil geometry.

Coil Number from Floor	Coil Pitch [cm]	Average Coil Height [m]
0 (offset)	3.44	
1	3.44	0.0516
2	6.87	0.1032
3	2.5	0.15
4	2.5	0.175
5	6.87	0.2219
6	6.87	0.2906
7	2.5	0.3374
8	5.15	0.3757
9	5.15	0.4272
10	2.5	0.4654
11	2.5	0.4904
12	2.5	0.5154
13	2.5	0.5404
14	2.5	0.5654
15	2.5	0.5904
16	2.5	0.6154
17	2.5	0.6404
18	2.5	0.6654
19	2.5	0.6904
20	2.5	0.7154
21	2.5	0.7404
22	2.5	0.7654
23	2.5	0.7904
24	2.5	0.8154
25	2.5	0.8404
26	2.5	0.8654
27	2.5	0.8904
28	2.5	0.9154

2.3 Instrumented System and Experimental Facility

The vapor compression system is instrumented at each state in the cycle to obtain the necessary parameters to calculate any other fluid properties at that state. Thermocouples are installed at the condenser inlet and outlet, expansion valve inlet, and the evaporator inlet and outlet. Absolute pressure transducers are

installed at the condenser outlet, expansion valve inlet, and evaporator inlet. Differential pressure transducers are installed across the condenser and across the evaporator. A power transducer is installed for measuring compressor power. A MicroMotion D012 Coriolis refrigerant mass flow meter is installed between the condenser outlet and the expansion valve. Instrumentation of the refrigerant mass flow meter required extending the liquid line. The modification is denoted in purple in Figure 2.2.

With the anode rod and the two heaters removed from the water tank, three threaded openings were opened. These openings were re-purposed to house three “thermocouple rods” for measuring the temperature of water at various locations. Each thermocouple rod is a sealed copper rod held by a threaded fitting with various thermocouples instrumented at various locations along the rod. The vertical thermocouple rod replaces the anode and has ten thermocouples. The two horizontal thermocouple rods replace the top and bottom heaters. Each horizontal rod has nine thermocouples.

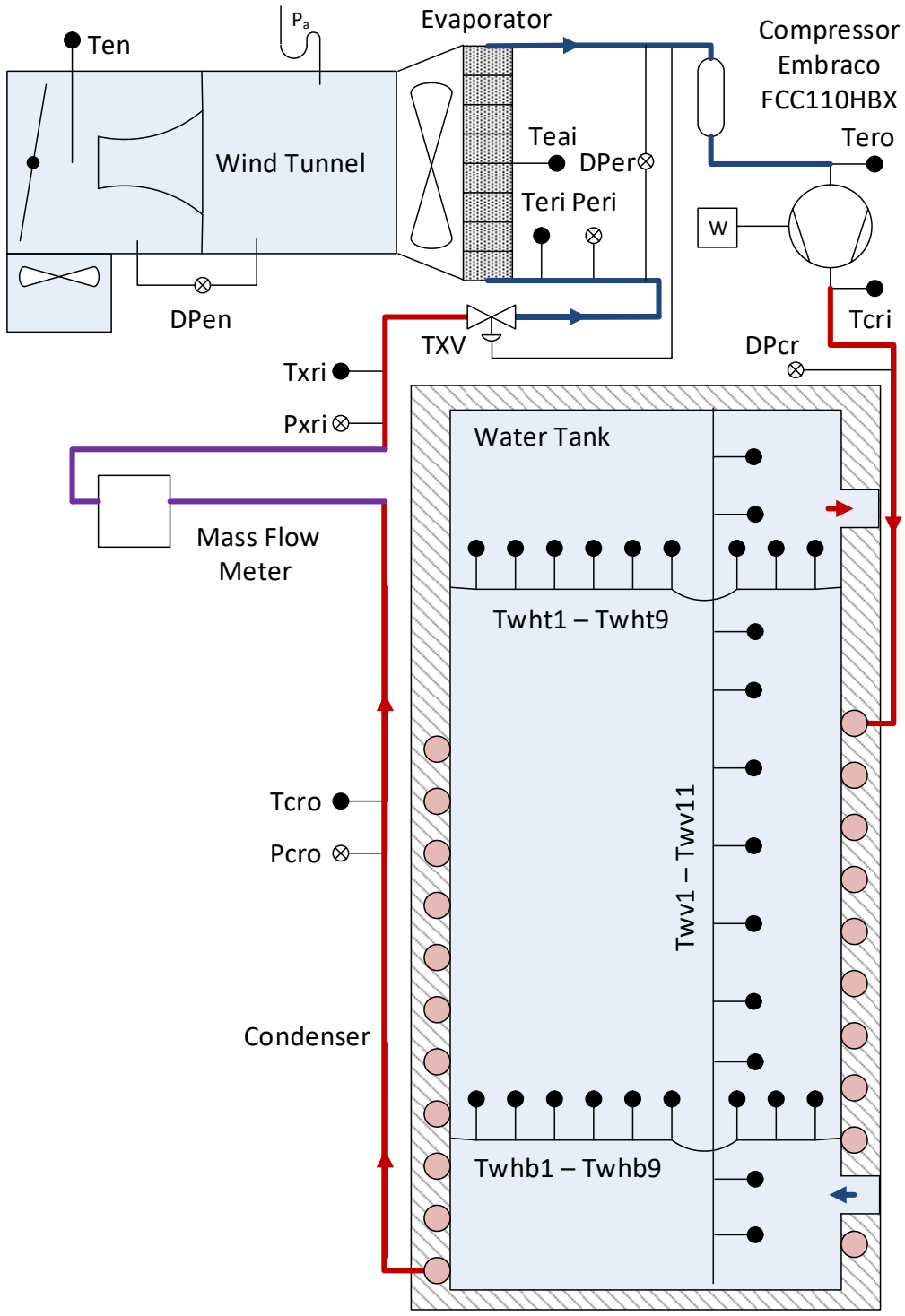

Figure 2.2: Instrumented system.

Air temperatures on either side of the evaporator are also measured with thermocouples. At the outlet of the evaporator, a wind tunnel is fitted to measure air flow across the evaporator. The wind tunnel consists of three sections: the pre-nozzle chamber, the nozzle, and the post-nozzle chamber. Knowing the nozzle geometry and pressure drop across the nozzle, conservation of mass and energy can be applied to determine the air flow velocities at the nozzle inlet and outlet. The blower fan in the post-nozzle chamber is used to prevent the nozzle flow restriction from loading the system. The adjustable vane in the post-nozzle chamber, when fully closed, will cause the pressure in the pre-nozzle chamber to drop below the ambient air pressure. As a result, the vane is set to a position such that the pressure in the pre-nozzle chamber matches the ambient pressure to ensure that the wind tunnel has no effect on the system operation.

Experiments are conducted in an environmental chamber in which ambient temperature is controlled to maintain a constant evaporator air inlet temperature.

Figure 2.3: Experimental facility in ACRC Mechanical Engineering Lab at the University of Illinois Urbana-Champaign.

CHAPTER 3. EXPERIMENTAL STUDY OF HEAT PUMP WATER HEATER SYSTEM

3.1 Experimental Overview and Methodology

Performance of vapor compression systems depends on the heating and cooling capacities at the heat exchangers, which are strongly influenced by the properties of the fluid mediums transfering heat (i.e. temperature, velocity, pressure). In the case of heat pump water heaters, particularly, these conditions never achieve a steady state due to the transient nature of residential end-use applications in the residential building and typical water demand schedules (i.e. human consumption). For example: temperature and velocity of water in the tank, ambient temperatures in the environment can change with the weather, and water draw during operation would all affect and contribute to the heat transfer and the performance of the system.

For the purposes of this investigation, it is imperative to simplify the experimentation to maximize repeatability, reduce noise for non-design related parameters, and enhance contrast in system performance metrics as relevant parameters vary.

For the subsequent experiments, the ambient temperature of the environment is provided by the environmental chamber via PID control. Water draw during system operation will not be considered. Also, the experiments will mostly focus on the worst-case but realistic mode of operation that is a full water tank warm-up from cold "city" water. This would approximate system operation after a short period of heavy demand, such as weekday mornings. As the water in the tank heats from cold to hot, the system will experience a wide range of operating conditions, which will be particularly useful in the validation of any analytical model.

3.2 Standard Operating Procedure

In addition to the instrumentation described previously, hoses and ball valves are fitted to the water tank hot exit (upper) and cold entry (lower) plumbing ports. The upper port is connected to the building water to support tank fill, and the lower port is connected to the drain. Due to fluctuations in building water temperature and to facilitate repeatability of experimentation, initial water temperature is set to 25°C. This is roughly room temperature and can be easily adjusted since the building water is generally colder. The environmental chamber PID control is utilized to add heat as appropriate to maintain an ambient temperature of 25°C inside the chamber. Also, no water is drawn from the tank during operation.

The system then continues to run on a "heat pump only" mode of operation. The system automatically stops once water temperatures, as measured

by the system's internal sensors, reach an electronic setpoint temperature of 52°C. The electronic setpoint adds another layer of repeatability to system operation as the same system shut-off conditions are met with each test. Generally, under this configuration, the system warm-up will span a duration of just over 5 hours.

Additional experimental work was done with different settings than described in this section. This work is documented in Chapter 7. For the purposes of developing a reliable analytical system model, the experimental methodology defined in this section was deemed to be most appropriate.

3.3 Typical System Performance

Using the experimental methodology described in Section 3.1, data is collected using the instrumentation described in Chapter 2. The processed data is presented below in the form vapor compression cycle plots for the refrigerant, system performance plots, and other relevant temperatures to describe the behavior at the condenser and water tank.

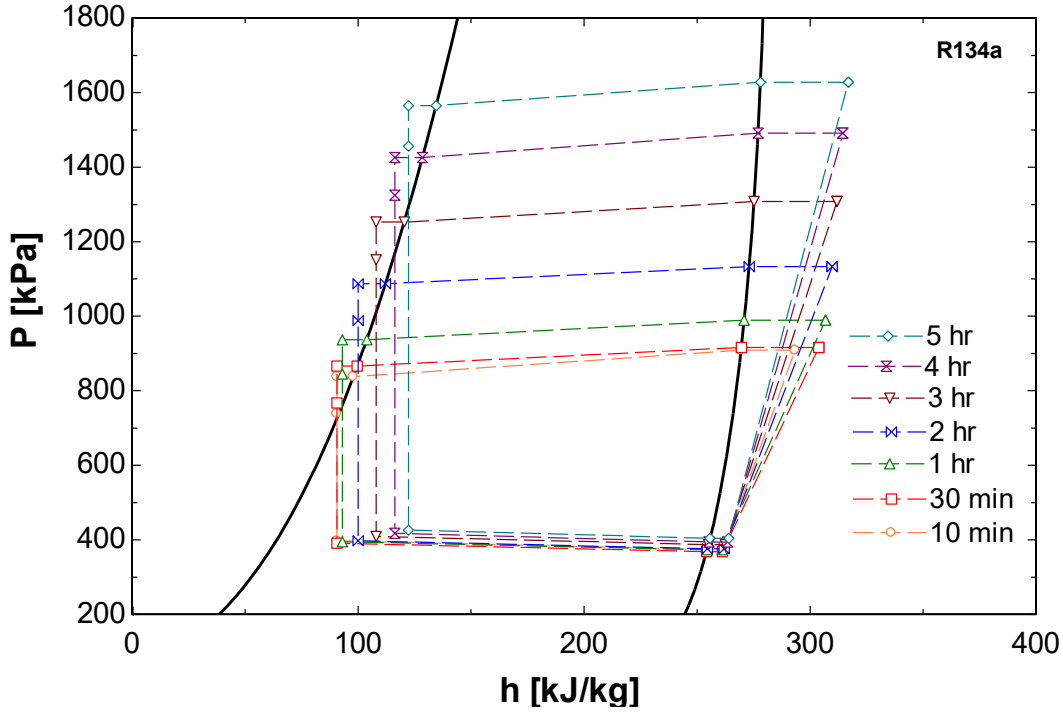

Figure 3.1: Plot of experimental system conditions (pressure-enthalpy) in full warm-up.

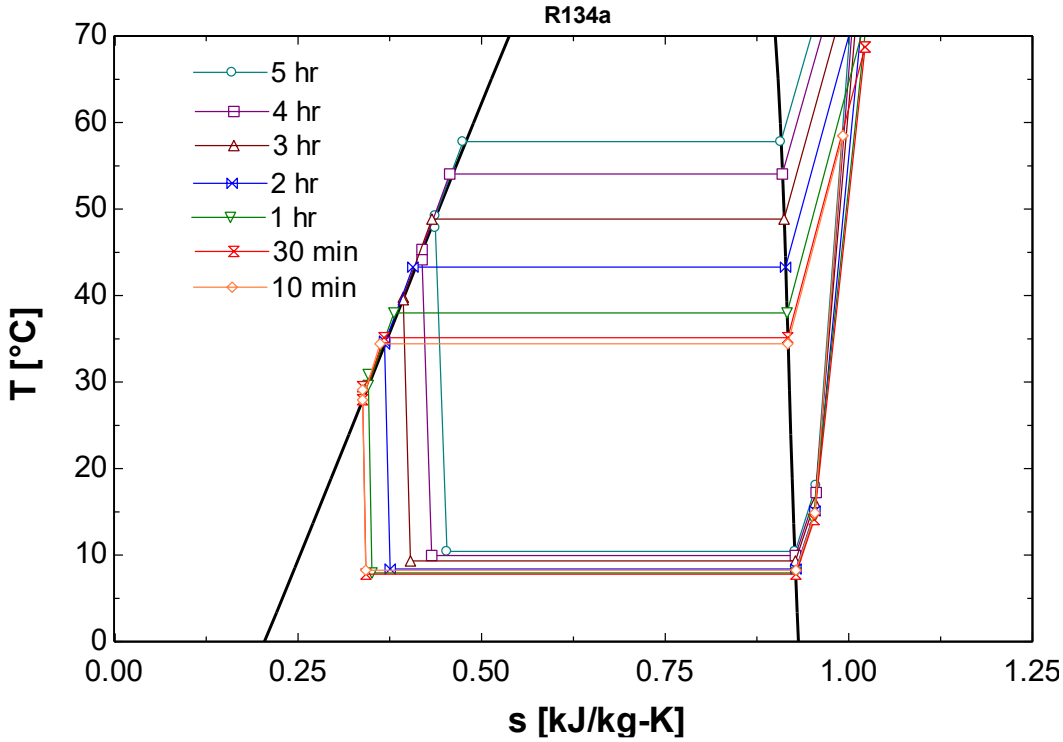

Figure 3.2: Plot of experimental system conditions (temperature-entropy) in full warm-up to emphasize change in temperature of water over during of system operation.

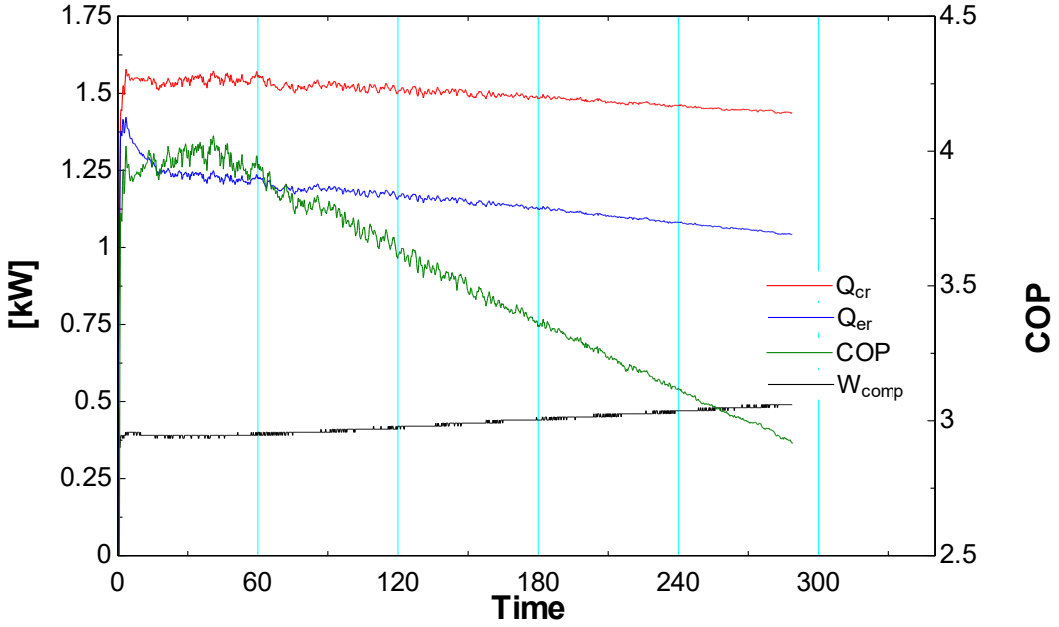

Figure 3.3: Experimental system capacity (condenser and evaporator) and efficiency in warm-up (time in minutes).

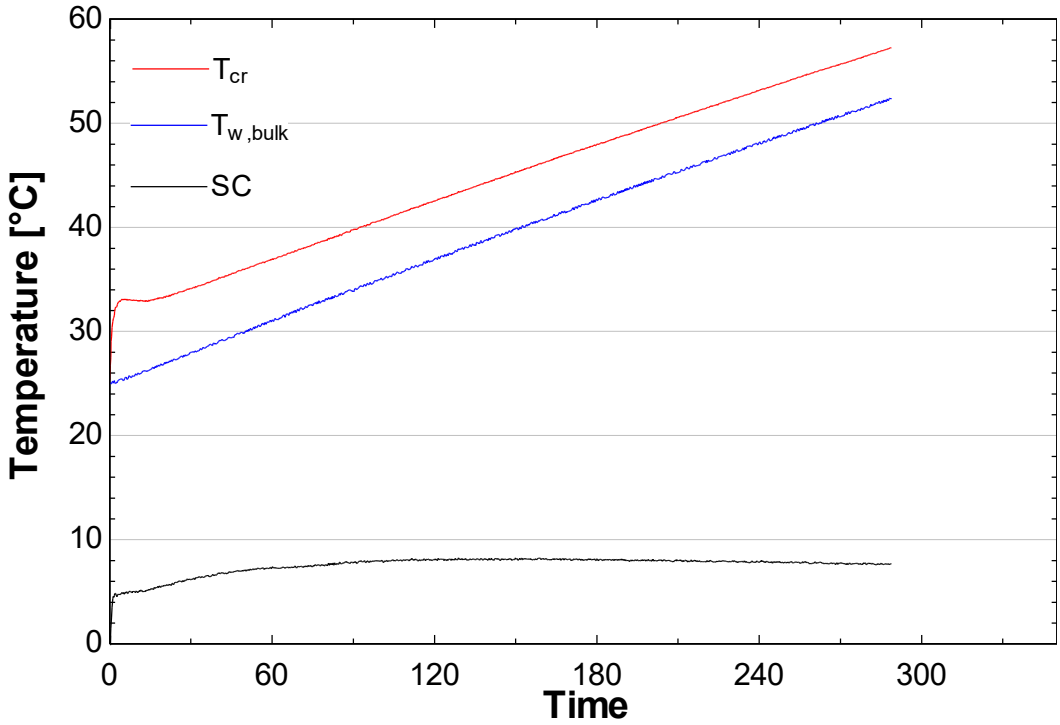

Figure 3.4: Condenser temperatures and subcooling in warm-up.

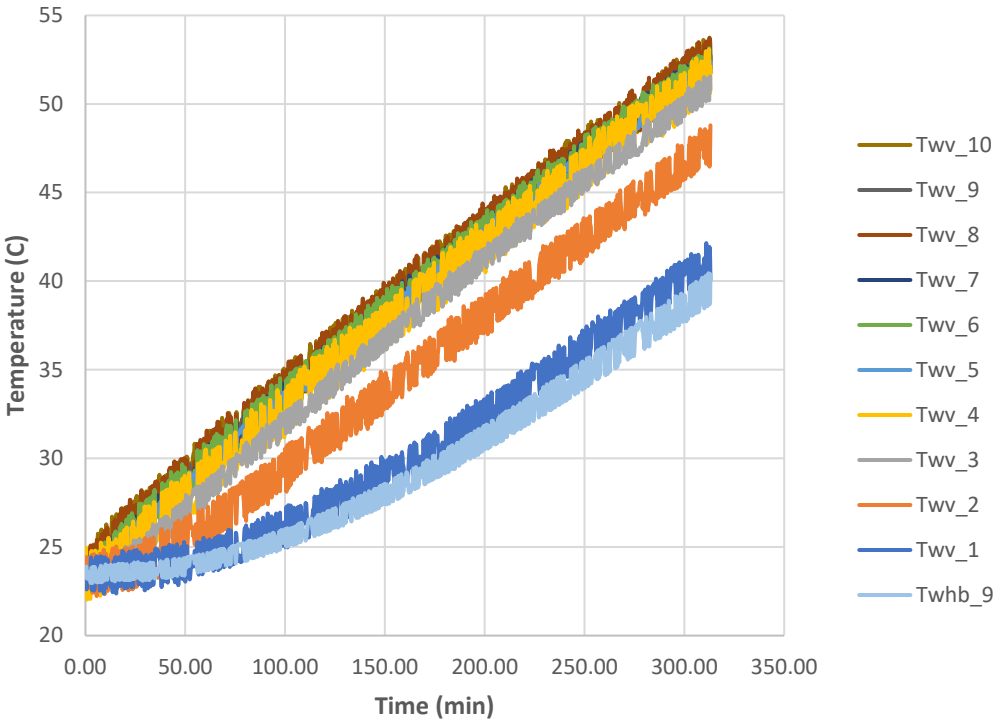

Figure 3.5: Water temperatures measured along vertical thermocouple rod.

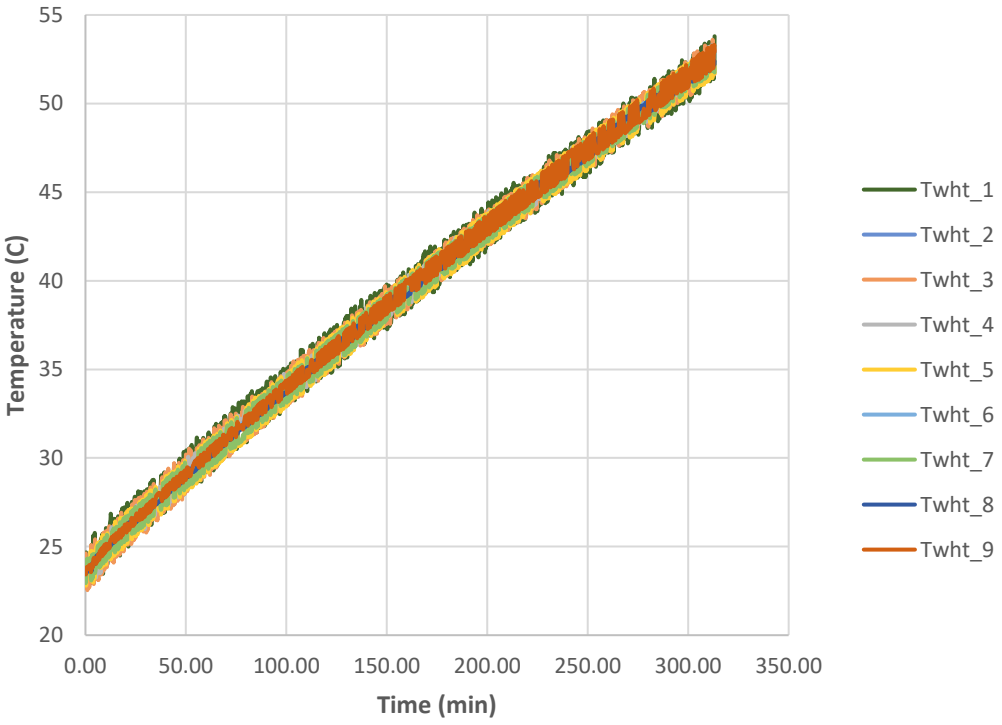

Figure 3.6: Water temperatures measured along upper horizontal thermocouple rod.

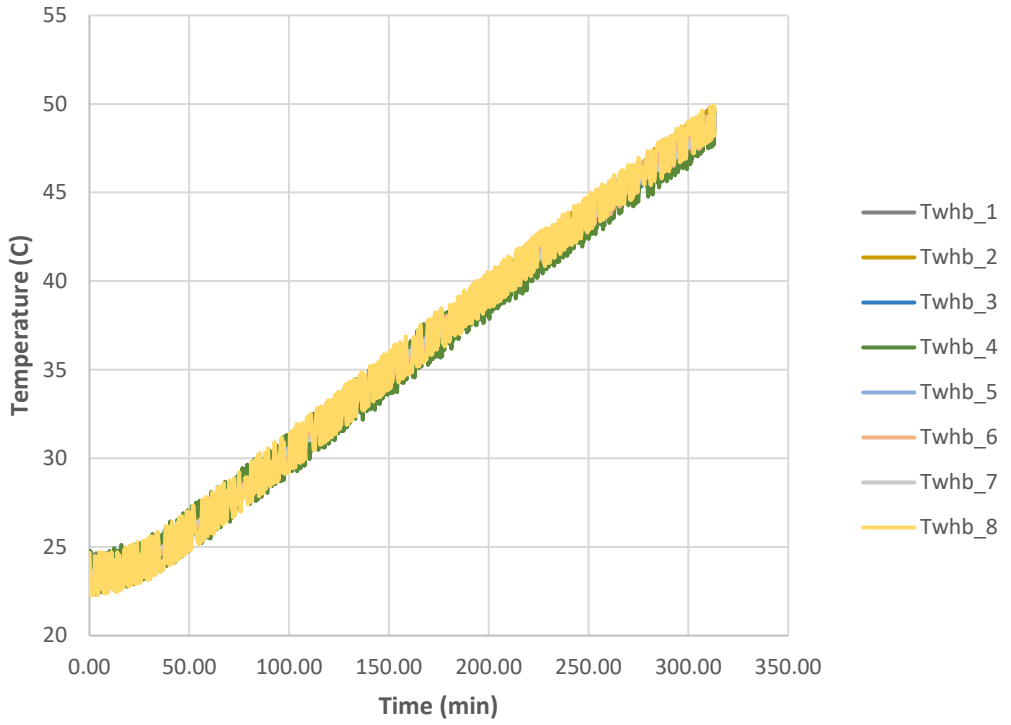

Figure 3.7: Water temperatures measured along lower horizontal thermocouple rod.

From Figures 3.1 and 3.2, the progression of the vapor compression system is apparent: a "quasi-steady-state" behavior as the system slowly changes as the temperature of the water in the tank steadily rises. Looking at the system COP in Figure 3.3, it is interesting to note that the system is most efficient at the start as water temperatures in the tank are the lowest. Figures 3.5, 3.6, 3.7 show the water temperatures over time. As expected, there are no observable differences in the temperatures measured in the horizontal rods. However, a vertical temperature stratification is in fact, evident and apparent, as shown in the data. This gradient in water temperatures will have a significant impact on the heat transfer characteristics of the condenser coils over time.

CHAPTER 4. CFD MODEL OF CONDENSER / COIL-WRAPPED WATER TANK

The first step in building the model is developing an accurate representation of the water tank and condenser as a heat exchanger. This will be achieved by creating a separate CFD model for the water in the water tank during the heating process using ANSYS Fluent software.

4.1 MODELING CONDENSER GEOMETRY

The condenser is a coil that wraps around the walls of the water tank. Superheated refrigerant is configured to enter the topmost coil and leave subcooled through the bottommost coil. The D-shaped cross-section of the coil tubes form a rectangular contact patch along the tank wall. To simplify the modeling, each coil is winding is flattened to as shown in Figure 4.1. Each flattened coil is spaced by respective coil pitch. This allows the CFD to be modeled in 2D (two dimensions) rather than 3D.

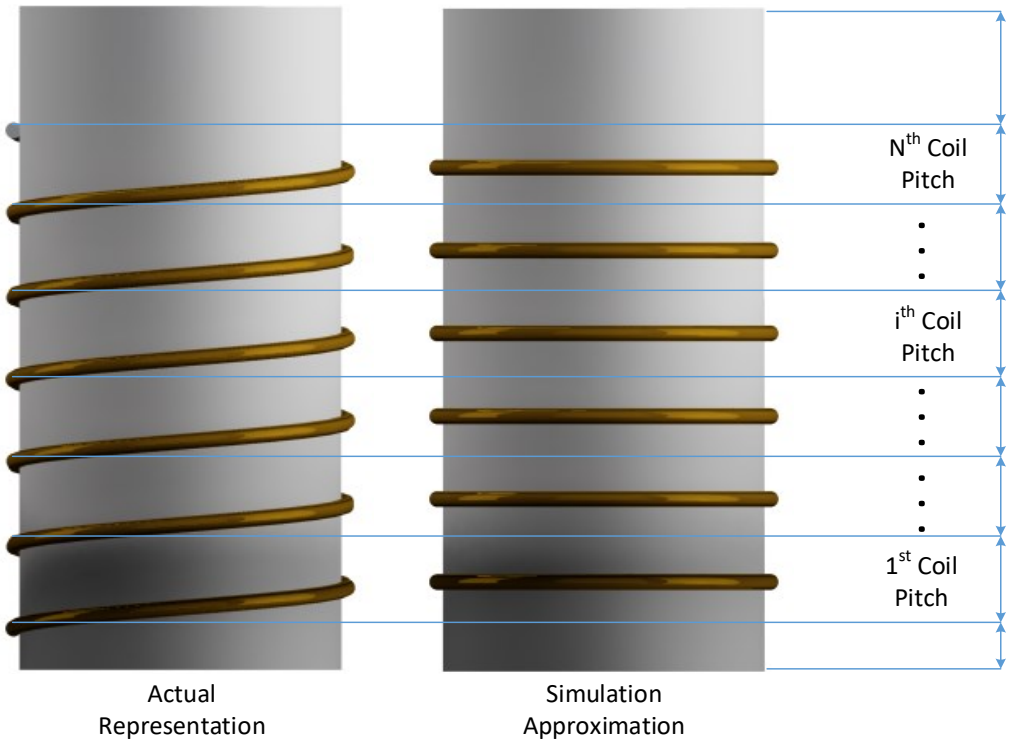

Figure 4.1: Adaptation of coil windings in modeling.

4.2 CFD Model Overview

For the purposes of this model, the water tank is simplified to a 2D axisymmetric geometry along the axial centerline of the water tank cylinder as shown by the meshed model in Figure 4.2.

Each coil is accounted for by a line segment that represents the corresponding section of the tank wall. As such, the length of each segment is the respective coil pitch of that corresponding coil. The model then assumes that for each segment, heat is passed to the water uniformly on the surface of the segment. The inputs to this model are the temporal heat flux profiles for each coil by Fluent's User Defined Function (UDF) feature. Key results of the CFD are

temperatures and velocities of the water at various positions inside the tank at various points in time. The use of CFD also allows for the accounting of bulk water temperature with respect to time during the simulation.

The transient or unsteady simulation was conducted with a second-order formulation and a pressure-based solver. SIMPLE scheme is used for pressure-velocity coupling. The Boussinesq approximation is used for computing density. Laminar flow is assumed to simulate the expected buoyancy-driven flow. The mesh is refined near the tank wall and tank top to more precisely capture the water recirculation during the heating process.

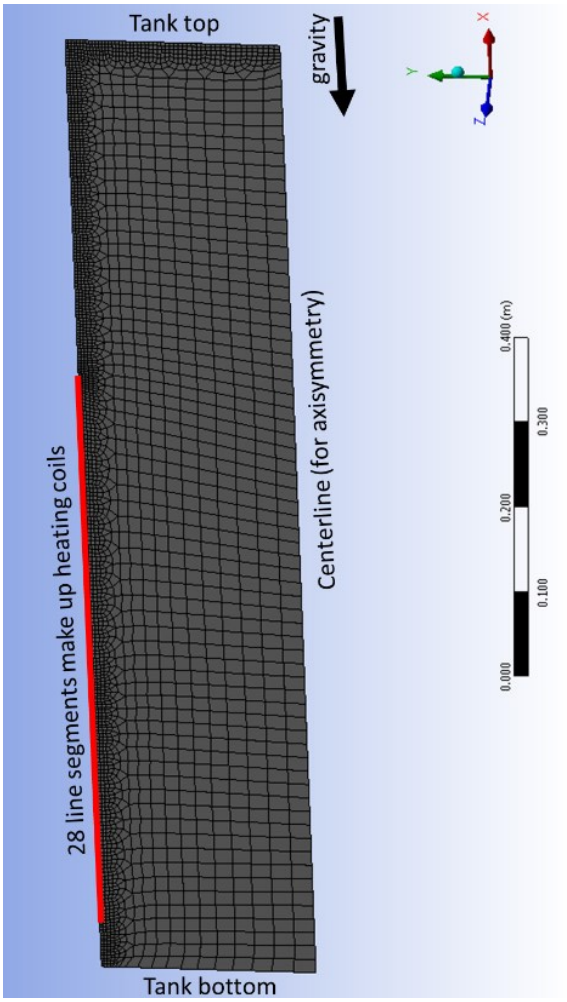

Figure 4.2: CFD mesh geometry.

4.3 Sample Results and Trends

A typical warm-up of the water in the tank follows a pattern similar to Figure 4.3 below. The water heated from the sides accumulates at the top and gradually mixes from top to bottom.

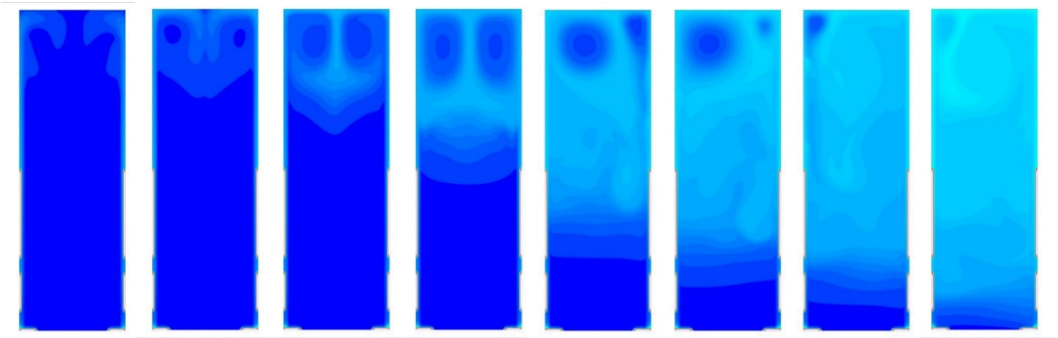

Figure 4.3: Example of natural convection fluid flow inside water tank during heating.

Below in Figures 4.4 and 4.5 are velocity pathlines and temperature contours of water after 1 hour of heating, respectively. These figures are shown as an example to illustrate to fluid motion and temperature during the system operation.

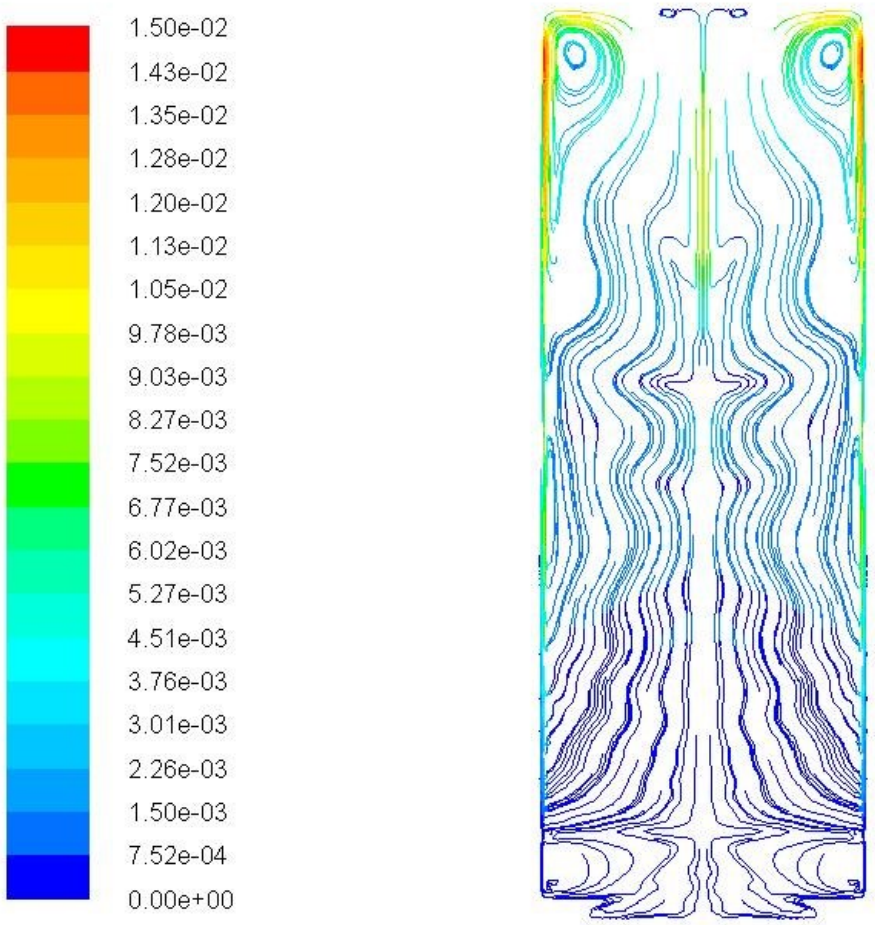

Figure 4.4: Velocity pathlines (m/s) of water in the tank at 3600s.

Two important observations from the velocity pathlines are high upward velocities near the tank wall and velocity magnitudes generally increasing with height along the tank walls. Furthermore, these observations can lead us to define a thickness for the upward flow stream near the tank walls. Over several CFD tests, this thickness was approximated at 2cm and would be incorporated in the system-level heat transfer calculations. Measurements of CFD results for near wall temperatures and velocities are stated as averages over this prescribed upward flow thickness in the context of determining heat transfer between the heated tank walls and the water.

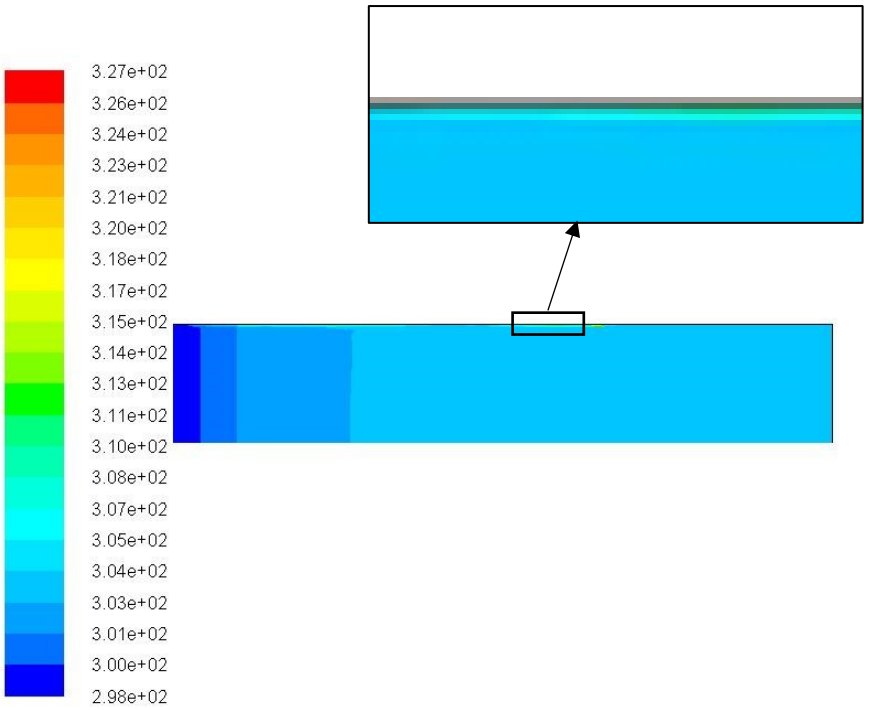

Figure 4.5: Temperature contours (K) of water in the tank at 3600s highlighting heated near-wall flow stream

Similarly, the temperature contours show higher temperatures in the upward flow stream near the tank walls due to the presence of the coils. Since the water is acting as the cooling medium for the condenser, water temperatures near the tank wall may affect overall system performance and condensing temperatures and pressures. At this point, the beginning of thermal stratification is also apparent in the form of a temperature gradient in the water tank.

CHAPTER 5. QUASI-STEADY TRANSIENT MODELING OF SYSTEM WARM-UP

5.1 Concept of Quasi-Steady Modeling Approach Linking CFD model and Steady-state System Model

Two primary behaviors form the basis of the modeling approach: First, a quasi-steady-state assumption is made due to the slow nature of the heating process as observed in Chapter 3. This allows the transient nature of the system to be modeled with reasonably large time intervals to reduce computational load. To capture the dynamic progression of the vapor compression cycle, the operation time is discretized into several steady-state time intervals by way of the quasi-steady-state assumption.

Second, the dynamic behavior of the water inside the tank driven by added heat over time as well as the resulting motion due to buoyancy forces as observed in the CFD model described in Chapter 4. This fluid motion is driven by the buoyancy effects of higher temperature fluid, with lower density, rising to the top of the tank by displacing lower temperature fluid. Consequently, an upward flow stream can be defined near the tank walls, and a downward flow stream can be defined in the remainder of the tank.

The overall vapor compression system model was built using Engineering Equation Solver (EES). A key output from this system model is the amount of heat transfer from each coil to the water in the tank.

For each steady-state time interval, the system model would require as inputs the spatial profiles for average near-wall velocity and temperature in the water tank in addition to the thickness of the upward flow stream. The remainder of the inputs is design parameters and the various specifications of the numerous system components. Certain parameters of interest are condenser coil geometry, refrigerant selection, and evaporator, and compressor sizing, etc. Once a validated linked model is developed, the selection of these parameters can be explored by way of sensitivity analysis under various modes of operation, i.e., full warm-up, high-temperature cycling, etc.

Figure 5.1 depicts the interdependency of the two models as they interface at the tank wall on the water-side.

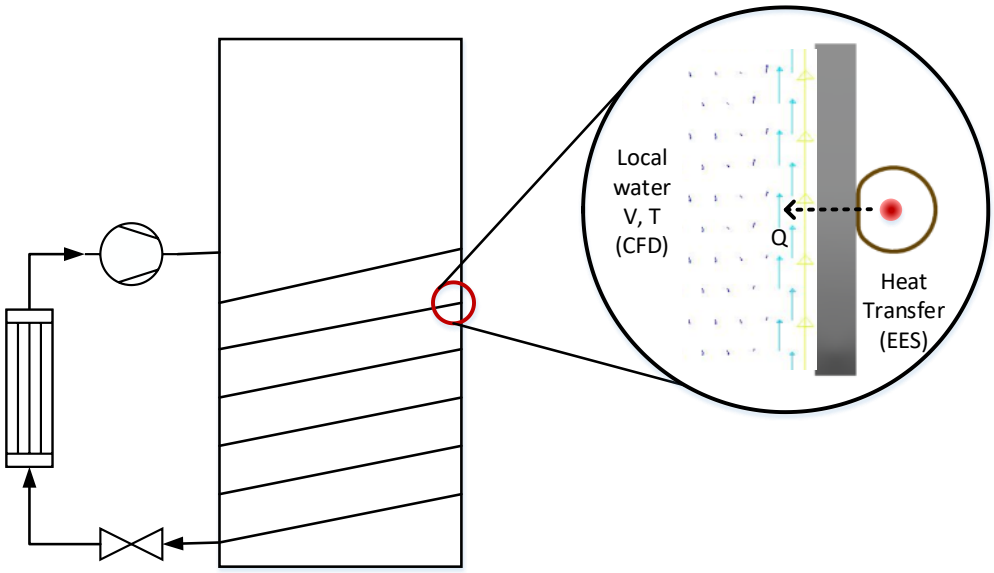

Figure 5.1: Interface of the CFD model and EES system model at water-side tank wall.

5.2 System Modeling Methodology and Details

The system model predicts refrigerant-side conditions on a finite volume basis throughout the length of the condenser coil. Moreover, the proposed linked modeling attempts to take into account the evolution of water-side temperatures and flowrates in time locally for each coil. This is accomplished by using local water-side information from CFD results to calculate instantaneous heat transfer rates, using the EES system model, for each coil at various points in time during which steady-state is assumed. The newfound heat transfer rates are then inputted back into the CFD simulation to obtain updated water-side information and to start an iteration process that would be taken to convergence.

The rate of heat transfer through the condenser is defined using the effectiveness-NTU methods represented by Equations 5.1 – 5.4 below for cross-flow heat exchange (Incropera et. al, 1990). As a result of the dynamic nature of the system, changing flow rates and temperatures on either the water-side or refrigerant-side will affect the respective heat transfer coefficients on either side. Consequently, the overall heat transfer coefficient, temperature difference, and in effect, the heat transfer rate is subject to change on this basis.

$$Q = UA\,\Delta T_{lm} = \varepsilon\, C_{min}\,\Delta T_{in} \tag{5.1}$$

$$\epsilon = f\left(NTU, \frac{C_{min}}{C_{max}}\right) \tag{5.2}$$

$$NTU = \frac{UA}{C_{min}} \tag{5.3}$$

$$C = \dot{m}\, c_p \tag{5.4}$$

In practice, the system model would be run for each nearly steady-state time interval. The model would march element by element on a finite-volume basis iterating until the system achieves convergence in mass and energy. As a result, heat transfer as defined above is calculated on an element-wise basis along with the parameters it depends on, notably U and A. ΔT_{in} would be known from the output of the previous element. To understand how these parameters are derived, it is useful to consider the system on an element level.

The condenser is defined to have N coils (Figure 4.1), and each coil is discretized into M elements as shown in Figure 5.2.

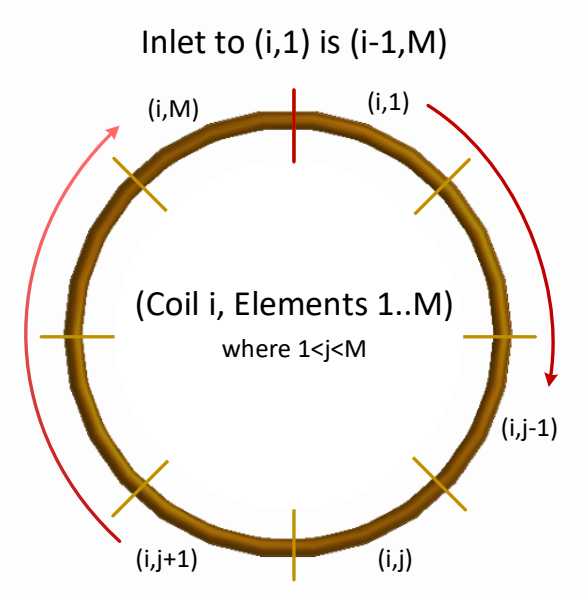

Figure 5.2: Discretization of each coil into elements.

Each coil element has a corresponding segment of tank wall and upward flow stream annulus of water inside the tank, as shown in Figure 5.3, due to buoyancy effects and natural convection.

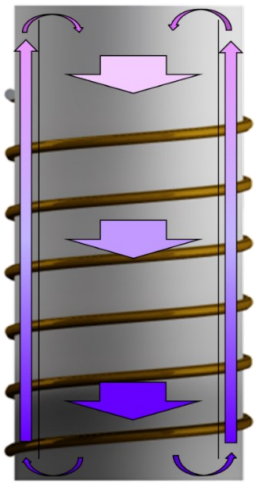

Figure 5.3: Natural convection inside the water tank.

As a result, the condenser comes together in three parts: the internal flow of refrigerant in the condenser coil, the laminar flow of water along the tank wall, and the thermal contact linking the coil and the wall. The modeling of each coil element is shown in Figure 5.4.

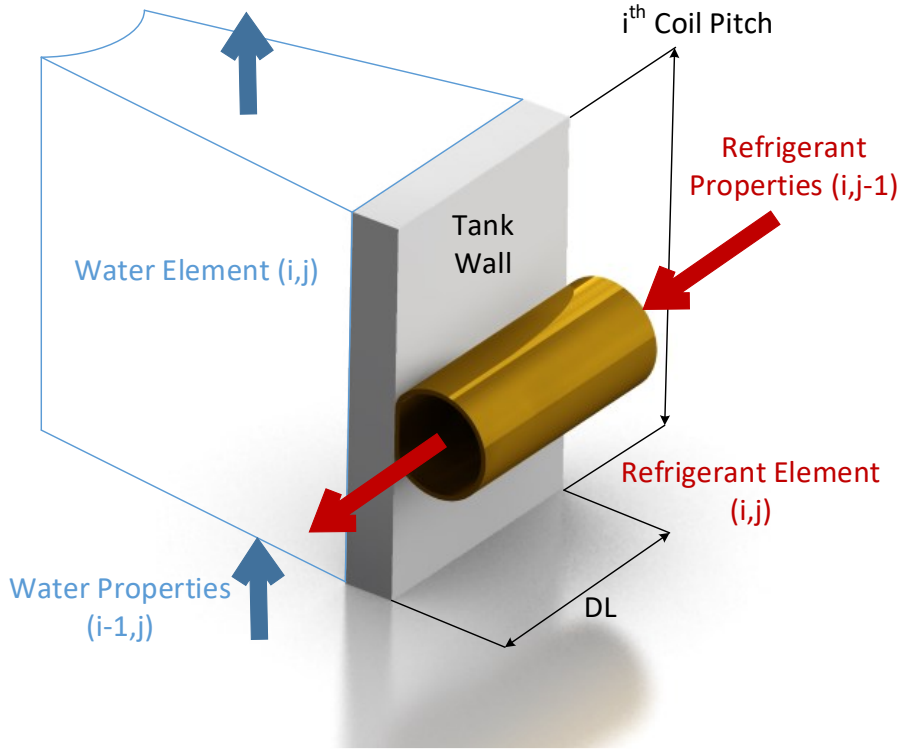

Figure 5.4: Typical coil element (i, j).

These three parts form the heat transfer path in the condenser and can be represented by thermal circuit in terms of their respective thermal resistances. Thus, UA, as a joint parameter, can be determined for this heat exchange as function of thermal resistances with the relationship in Equation 5.5 below.

$$UA = \frac{1}{R_r + R_c + R_w} \tag{5.5}$$

Next, the refrigerant coils and the water tank walls are each simplified as fins in external flow as shown in Figure 5.5. The fins are assumed adiabatic at the tip and the sides. The area of the fins can be determined by a product of the width of each marching element and either coil pitch (for the water side) or coil circumference (for the refrigerant side).

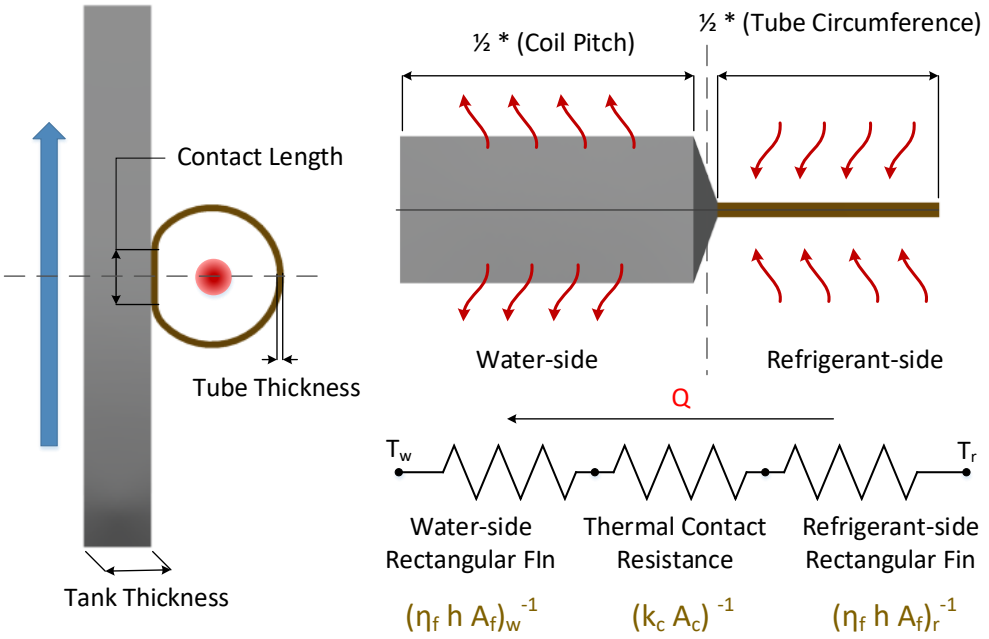

Figure 5.5: Element level modeling simplification and description of heat path.

Based on the representation above, the various thermal resistances are defined below in Equations 5.6 – 5.8.

$$R_r = \frac{1}{(\eta_f \, h \, A_f)_r} \tag{5.6}$$

$$R_c = \frac{1}{k_c \, A_c} \tag{5.7}$$

$$R_w = \frac{1}{(\eta_f \, h \, A_f)_w} \tag{5.8}$$

The value for contact resistance is estimated with generally available data on contact resistance. In reality, this value may also take on a dynamic behavior as contact pressure may change with the expansion and contraction of the refrigerant coils due to changing temperatures in the condenser. In this model, however, the thermal contact conductance will be approximated as a constant. Modeling this parameter as dynamic would require in-depth testing to obtain properties specific to this product and may only provide limited insight into the optimization of vapor compression systems.

The fin efficiencies are defined by Equations 5.9 and 5.10 where x represents the fin length and t represents the fin thickness.

$$\eta_f = \frac{\tanh\,(m \, L_c)}{m \, L_c} \tag{5.9}$$

$$m \, L_c = \left(x_f + \frac{t_f}{2}\right)\sqrt{\frac{2 \, h}{k_f \, t_f}} \tag{5.10}$$

The final components to evaluate are the heat transfer coefficients of the respective fluids. For the water in the tank, the flow regime is assumed as laminar external flow over a flat plate. In this case, the heat transfer coefficient is determined using Equations 5.11 – 5.13.

$$h_w = \frac{Nu\, k_w}{z_{cp}} \tag{5.11}$$

$$Nu = 0.664\, Re^{1/2}\, Pr^{1/3}, \quad where\ \mathrm{Pr} \geq 0.6 \tag{5.12}$$

$$Re = \frac{\rho\, V\, z_{cp}}{\mu} \tag{5.13}$$

For the refrigerant side heat transfer coefficient, as is typical with any modeling approach of a heat exchanger in a vapor compression system, the system model must first determine the phase and flow regime of the refrigerant and apply the corresponding correlations. For heat transfer coefficients, Gnielinski (1976) correlation is used for single phase R134a along with Dobson and Chato (1998) correlation for two phase flow. Additionally, Churchill (1977) correlation used for internal flow friction factor, Souza (1995) correlation used for two phase pressure drop, and Zivi (1964) correlation used for void fraction.

To evaluate a different configuration of the condenser coils (e.g. condenser coils submerged in the water), the condenser model described above can be easily refactored by deriving a new UA parameter based on a new thermal circuit. A selection of EES code specific to the condenser UA modeling provided in Appendix C.

The remaining components of the system model are typical and are modeled using existing functions with the corresponding geometry of the actual part as an input. The compressor model is modeled as a typical fin-and-tube heat exchanger as described in Section 2.2. Additionally, for the compressor, empirical curves for isentropic and volumetric efficiencies were provided by the manufacturer. These curves are inputted into the system model as functions of the

pressure ratio of compressor discharge pressure to suction pressure. The thermal expansion valve is modeled as an isenthalpic process.

Once a converged solution is achieved in the system model, the system is represented as a steady-state cycle for a specific time interval along heating and cooling capacities and a COP for the system. In this case, the specific heat flux contributed by each coil to the water tank in the condenser is also of interest and can be tallied accordingly based on element-wise data. The resulting array of data serves as a piece-wise spatial heat flux function discretized by condenser coil and is a critical input for advancing the CFD simulations.

5.3 LINKING ALGORITHMS

As a consequence of the required inputs of both models, linked modeling would allow for simulations to be representative of real system operation. To implement the linked modeling, an iteration procedure is needed that feeds heat flux profiles to the CFD model from the system model, and velocity and temperature profiles to the system model from the CFD model.

The first linking algorithm is based on dividing iterations in the space domain as shown in Figure 5.6. In this case, the space domain constitutes as the coil architecture.

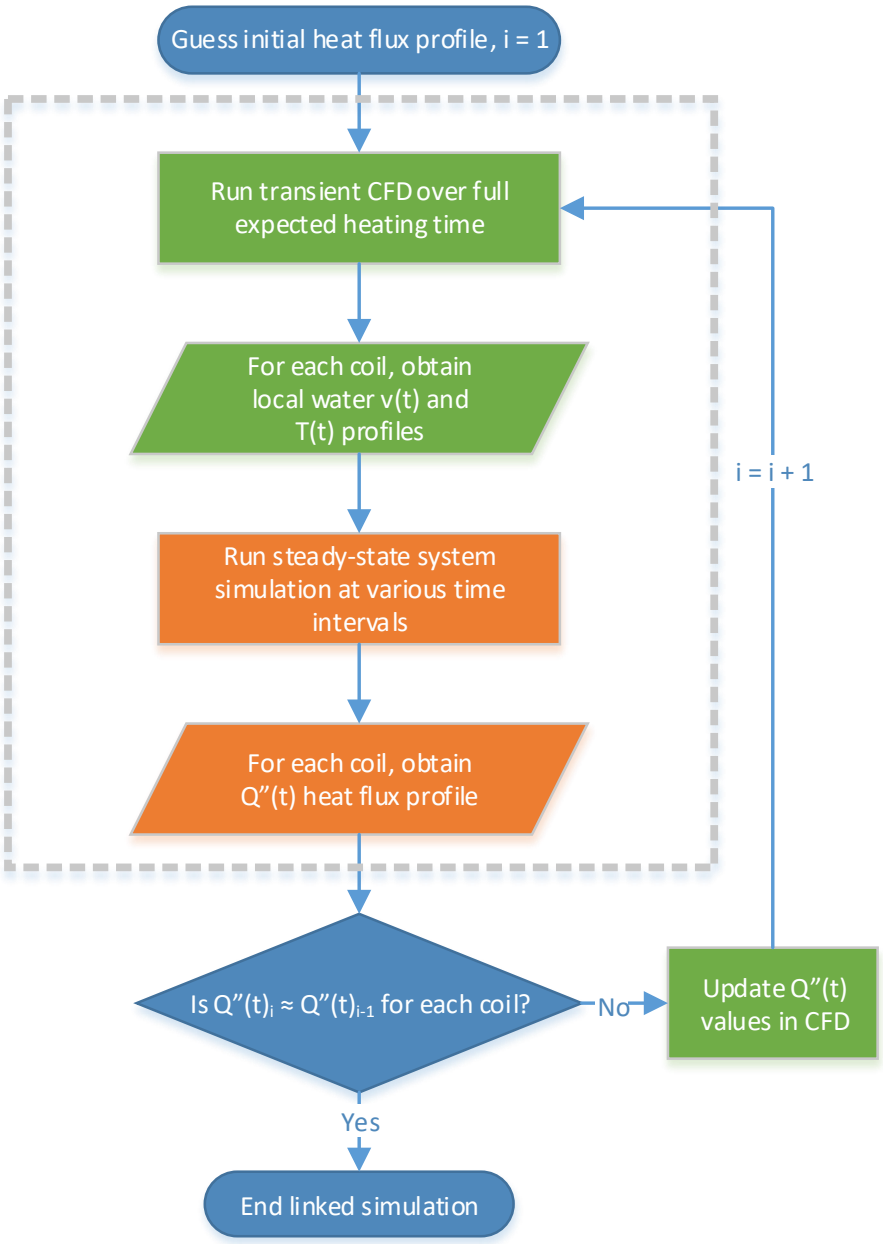

Figure 5.6: Linking algorithm 1, iteration in space.

In this model, a transient CFD is run for the full expected duration of the water heating process. Then, the CFD results are discretized into various time intervals, and the steady-state system model is run for each of the time intervals. The result of each iteration is an updated heat flux profile as a function of time for each coil. The heat flux profiles are then updated in the CFD, and the iterations

repeated again until the residuals of the profiles after each iteration begin to approach zero.

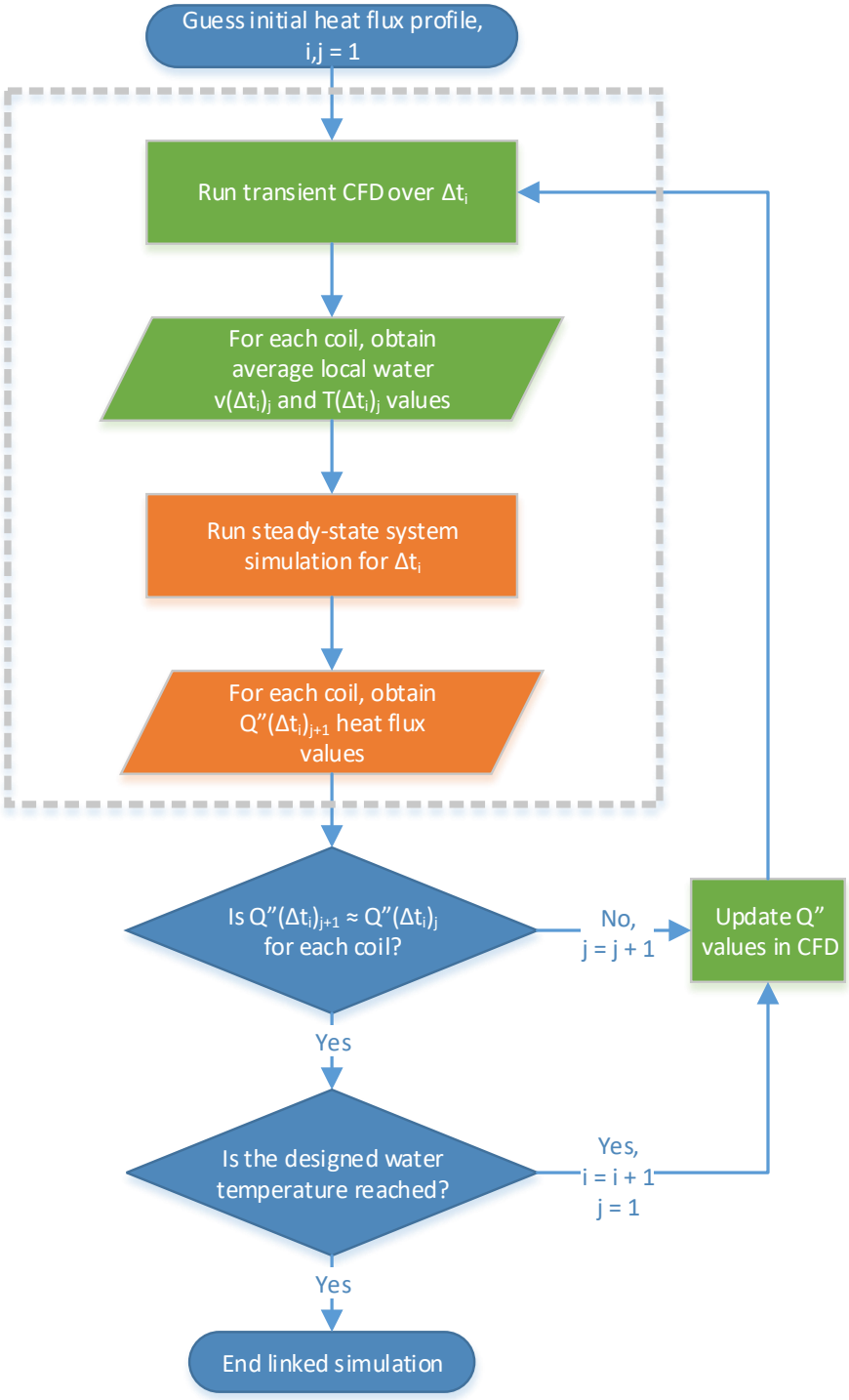

Figure 5.7: Linking algorithm 2, iteration in time.

The second linking algorithm is based on dividing iterations in the time domain as shown in the flowchart in Figure 5.7. The essence of this model is first to select a steady-state time interval for which the system model can produce a heat flux profile, and then to run a transient CFD simulation within that time interval that will produce temperature and velocity profiles. In each iteration, the respective profiles are passed between the respective models. Once the residuals of the profiles after each iteration begin to approach zero, iteration for current time interval can stop and begin for the next time interval.

The linked modeling will thus produce functions in time of heat flux, water velocity, and water temperature for each coil.

5.4 Implementation in Practice

Eventually, in practice, the converged solution of either algorithm would yield identical results. One should choose the method that can execute in the shortest duration. In this case, linking algorithm 1 was the optimal choice for a few reasons. First, CFD runs are long in duration and can be set up to run without supervision after which, the steady-state system models can iterate solutions in minutes based on the velocity and temperature profile inputs. The resultant heat flux profiles from the system model can then be fed back into CFD to kick off another long duration run. Second, by iterating over a series of time increments per algorithm 2, the number of manual data transfer events increases significantly and requires continuous attention quickly becoming a tedious process.

Algorithm 1 can be further optimized by not running the CFD for the full expected heating time during the initial iterations. This is justified because it is safe to assume that the model will require several iterations to converge. Therefore, there is no point to iterating a solution for hour 5 (system time) when the solutions through hours 1 and 2 are not fully developed.

The process for manual data transfer interfacing required to complete the linking will be outlined as follows for reference. Starting with the ANSYS Fluent CFD model, the first step is to sample the near wall velocity and temperature of the water along the height span of the condenser coils. In this case, 5 points were sample to build a profile.

Table 5.1: Sample velocity and temperature data points from CFD for a given time.

Position	Height [m]	Velocity [m/s]	Temperature [C]
Coil 1	0.0516	0.0069	20.935
Coil 7	0.3374	0.0163	21.355
Coil 14	0.5654	0.0212	21.6
Coil 21	0.7404	0.0254	21.77
Coil 28	0.9154	0.0294	21.82

From a dataset similar to Table 5.1, curve fits can be built to develop a continuous profile for temperature and velocity as a function of coil height.

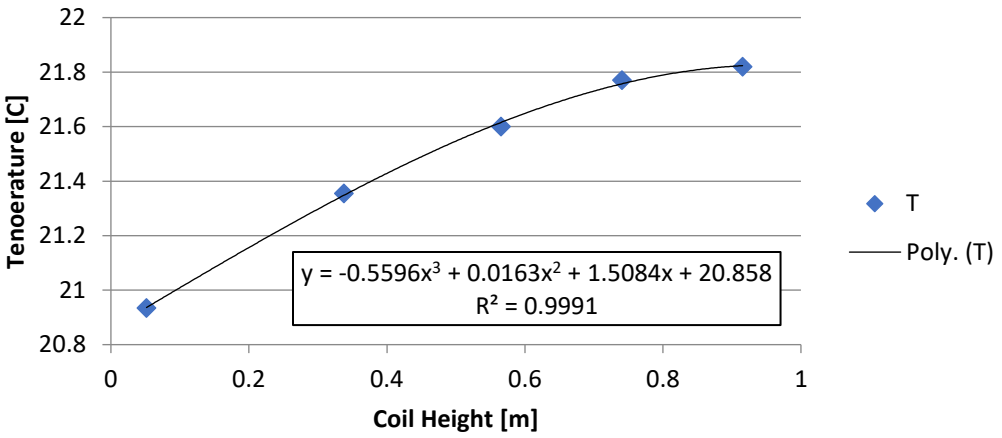

Figure 5.8: Sample temperature profile as a function of coil height.

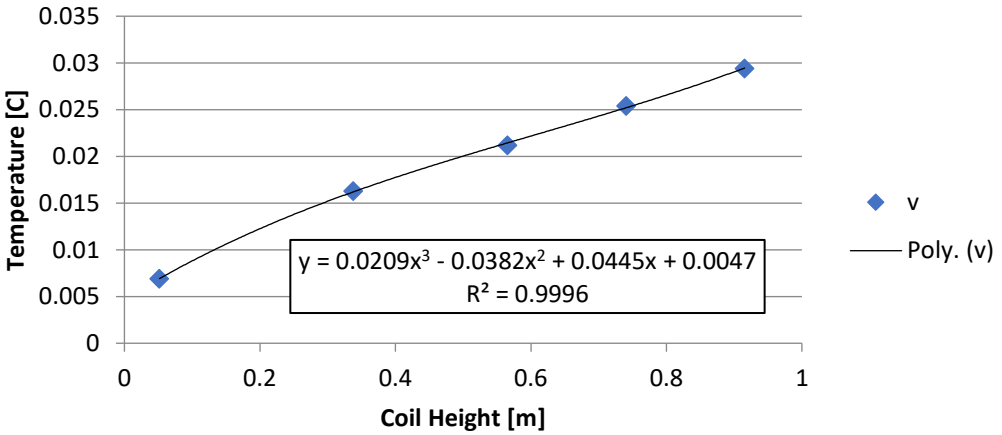

Figure 5.9: Sample velocity profile as a function of coil height.

To reiterate, the values presented in this section are an example to effectively convey the methods in practice. Additionally, these curve fits would be sampled at multiple times through the CFD run. In practice, the time intervals used are as follows: 2 minutes, 20 minutes, 1 hour, 2 hours, and hourly thereafter as needed.

Then, for each time interval, the EES system model would be run with the corresponding temperature, and velocity profiles provided as inputs either in the

form the curve fit polynomial or a look-up table with values calculated for each coil based on the curve fit polynomial.

The steady-state system model will solve the for the properties of the refrigeration cycle on an element-wise basis for each point in the system. In addition to an output system performance data such as heating and cooling capacities, compressor work, and property plots, the EES model is configured to also aggregate element-wise heat flux in the condenser coils into per coil basis in the form of an array.

Thus, a per coil heat flux array is generated for each time interval specified earlier. These arrays are then assembled in a template UDF file (.c format). The code for the Fluent UDF is provided in Appendix B. The UDF files contain a series of identical functions (one for each coil) that will compute the instantaneous heat flux during the CFD run based on interpolation for the data in the arrays.

CHAPTER 6. MODEL RESULTS AND VALIDATION

This section will consist of a presentation of simulation results using the modeling techniques designed in Chapters 4 and 5 and a comparison to experimental data collected in Chapter 3.

6.1 Model Results and Iterations over Time

The simulation results in this section are presented in the form of near-wall velocities (Figures 6.1 and 6.2) and near-wall temperatures (Figures 6.3 and 6.4). Results from iteration 2 will also be shown along with results from iteration 5 to show the progression of the data through the linked modeling.

The velocity data shows a pattern of acceleration from the bottom of the tank to the top as the subsequent heat transferred from each coil increases the buoyancy effect on each unit volume of water.

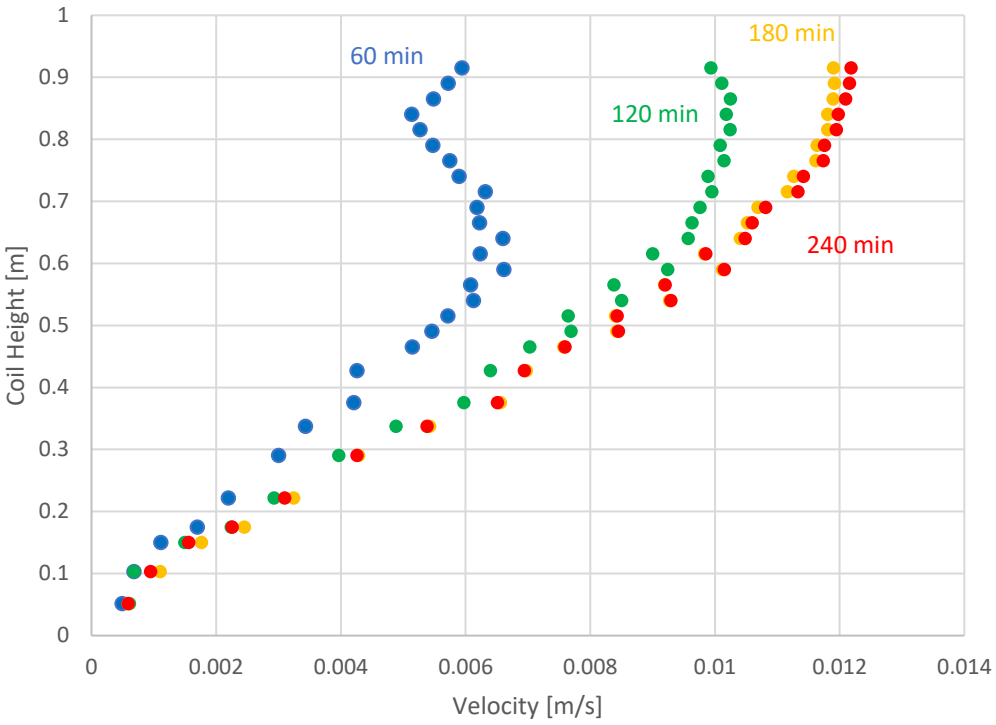

Figure 6.1: Simulated near-wall velocities of water over time at each coil height at iteration 2.

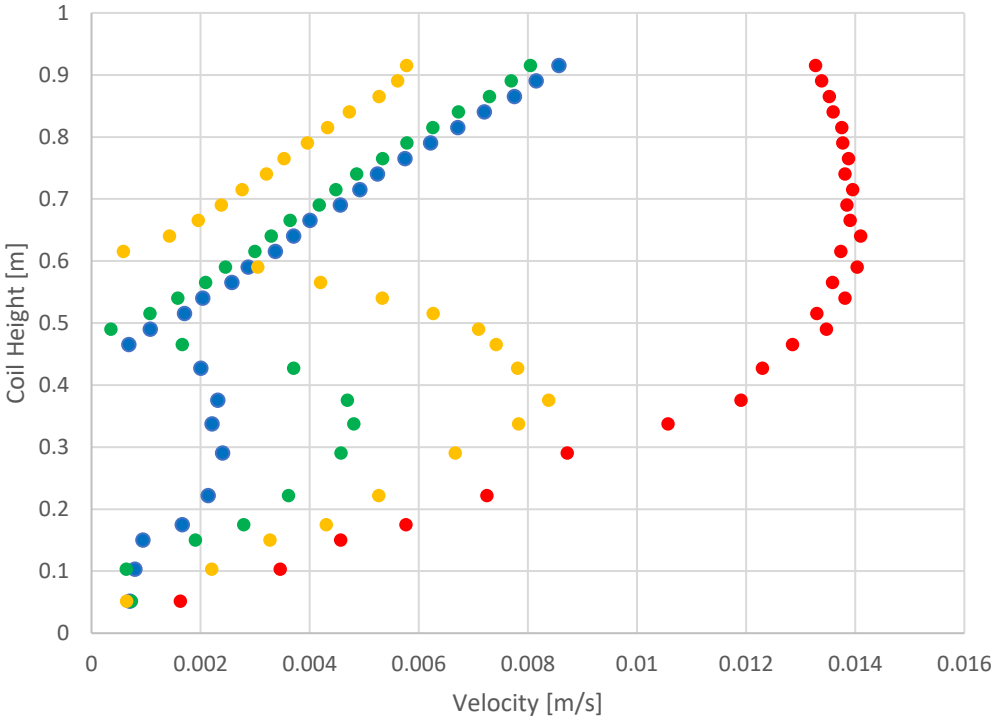

Figure 6.2: Simulated near-wall velocities of water over time at each coil height at iteration 5.

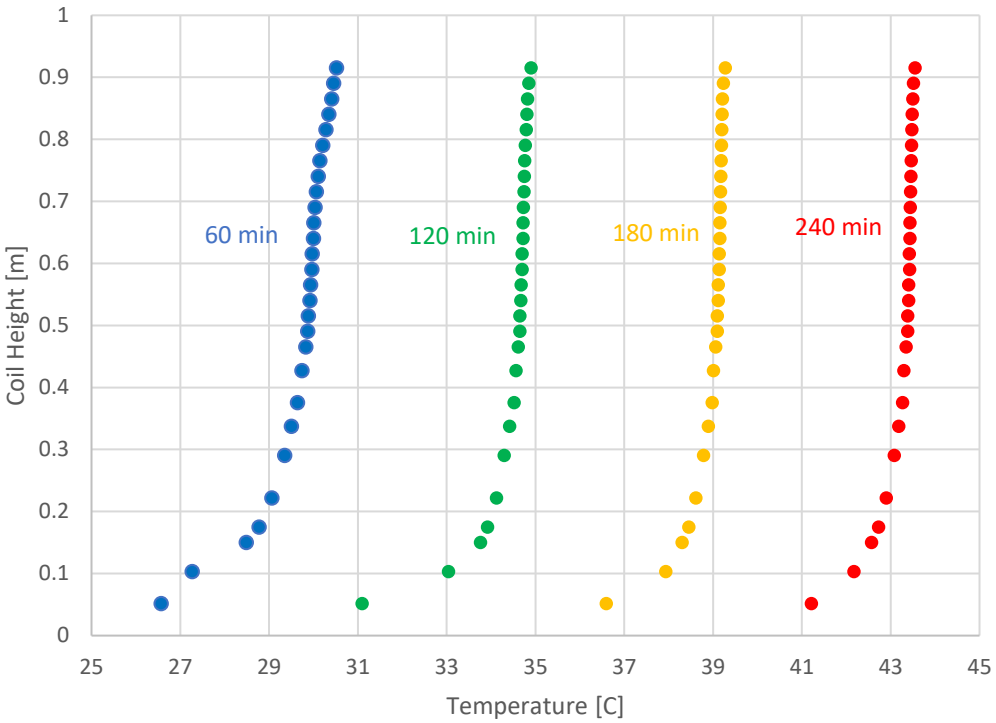

Figure 6.3: Simulated near-wall temperatures of water over time at each coil height at iteration 2.

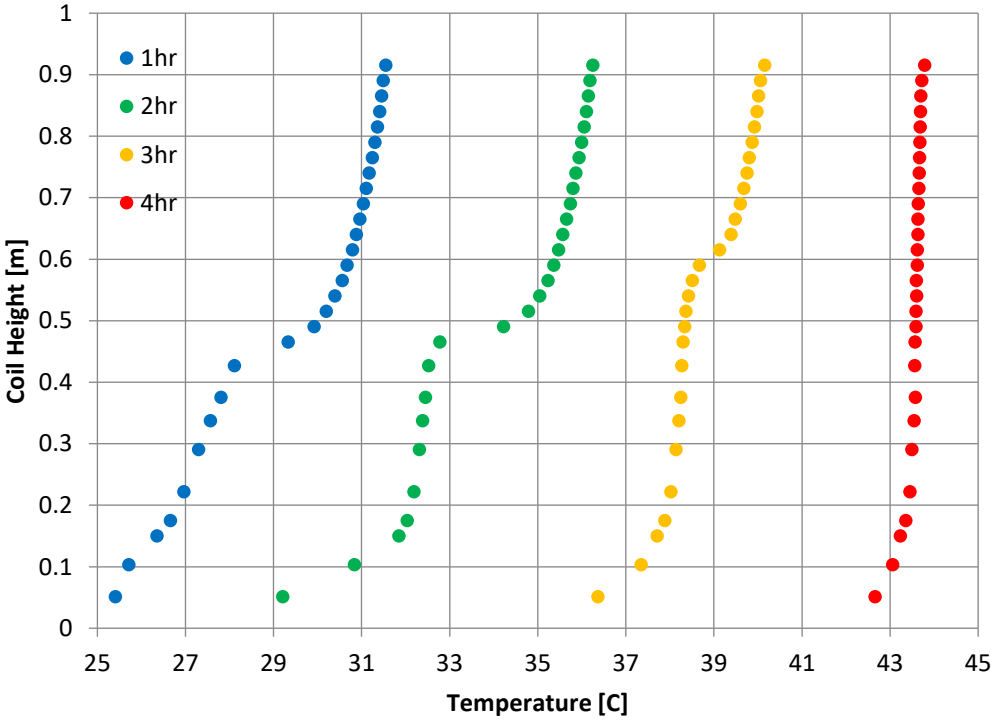

Figure 6.4: Simulated near-wall temperatures of water over time at each coil height at iteration 5.

The temperature plots start developing a more pronounced stratification as the simulation iterations progress.

6.2 Water Temperatures Predicted vs. Measured

Next, the temperature stratification of the water in the tank is compared against that from the physical tests. The simulation results are compared against experimental results from two different refrigerant charges: the nominal charge represented by 768g and a lower charge of 649g. These results are sampled from a refrigerant charge study detailed in Chapter 7.

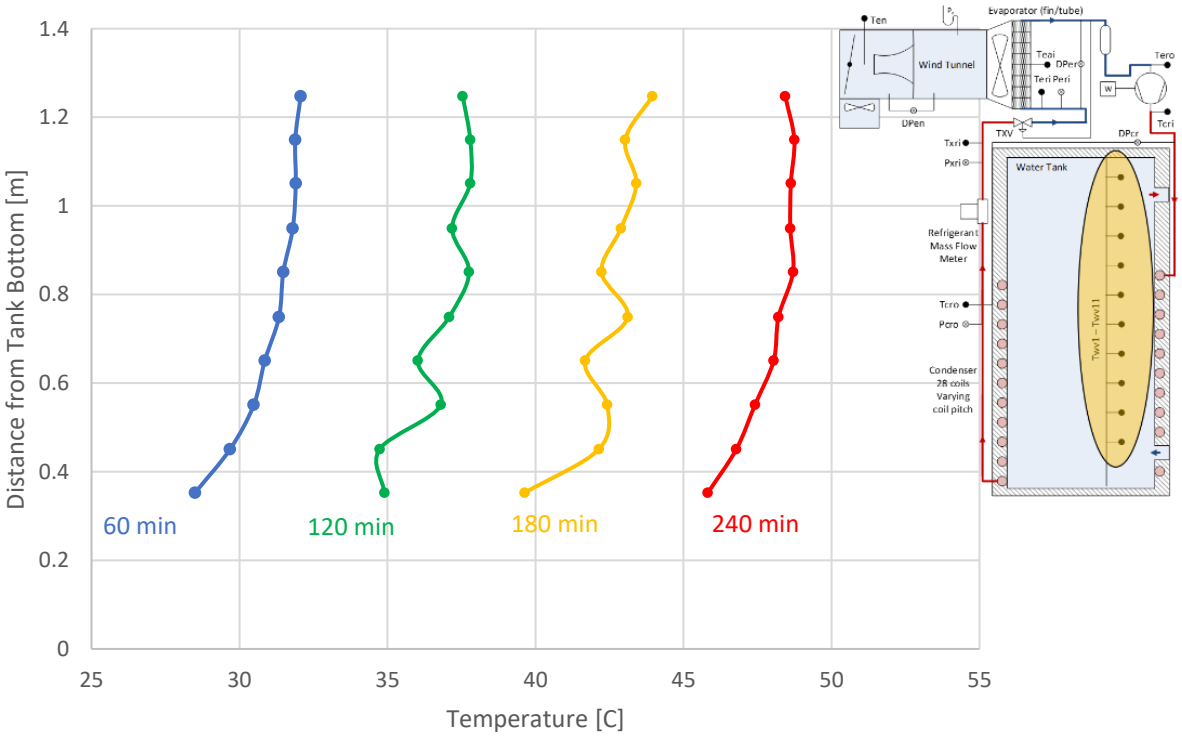

Figure 6.5: Measured water temperatures for system at nominal refrigerant charge of 768g.

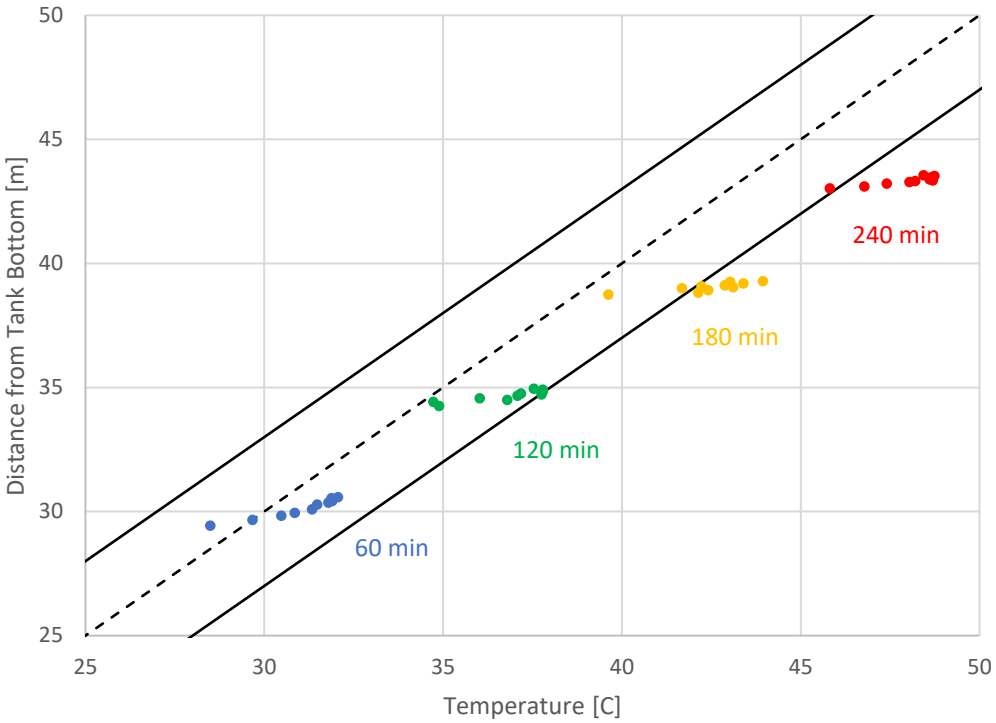

Figure 6.6: Predicted water temperatures (at iteration 2) vs. measured (refrigerant charge = 768g).

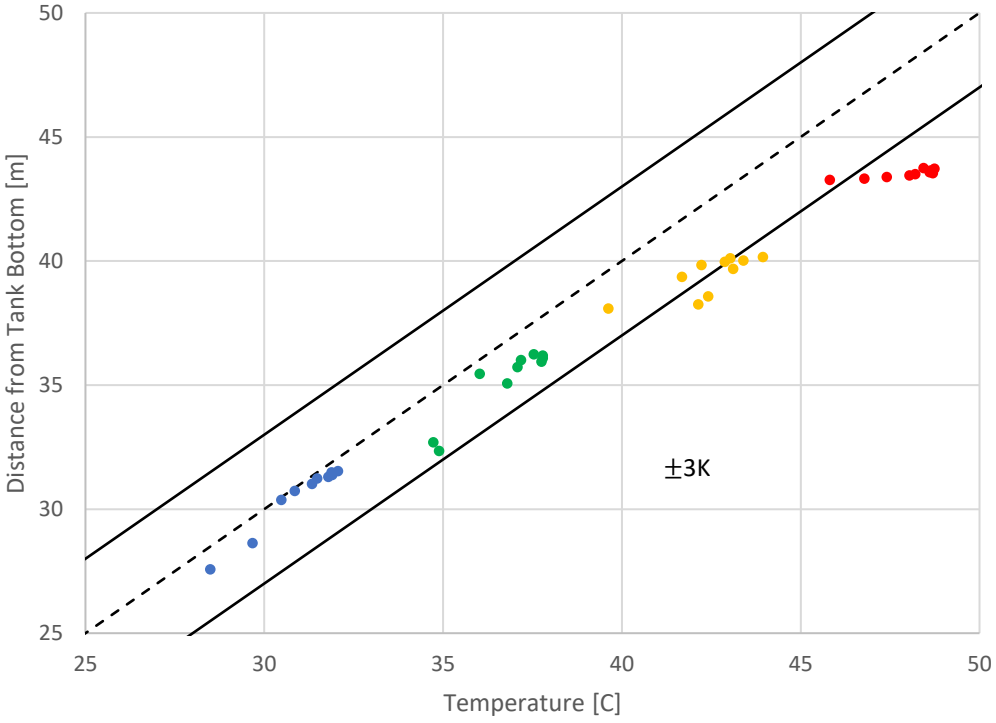

Figure 6.7: Predicted water temperatures (at iteration 5) vs. measured (refrigerant charge = 768g).

The experimental results for a nominal charge are shown in Figure 6.5. This is compared to simulated water tank temperatures at iteration 2 (Figure 6.6) and iteration 5 (Figure 6.7). It is apparent that as the iterations in the linked modeling progress, more accurate alignment and stratification of temperatures begin to develop in the simulation. Most likely, several more iterations would have helped in further developing the results. Another observation is that the simulated results are consistently underpredicting the water temperatures. This may be a consequence of too few iterations, but it could also a consequence of the system model under predicting refrigerant mass flow. As a result, measured results at a refrigerant charge of 649g are presented in Figure 6.8 and compared against the simulation results.

Looking at a comparison with iteration 5 in Figure 6.10, there is a significant improvement in correlation at 120min and 180min, yet 240min is relatively unchanged. This would suggest that a continuation of model iterations would be the immediate next step in furthering the model.

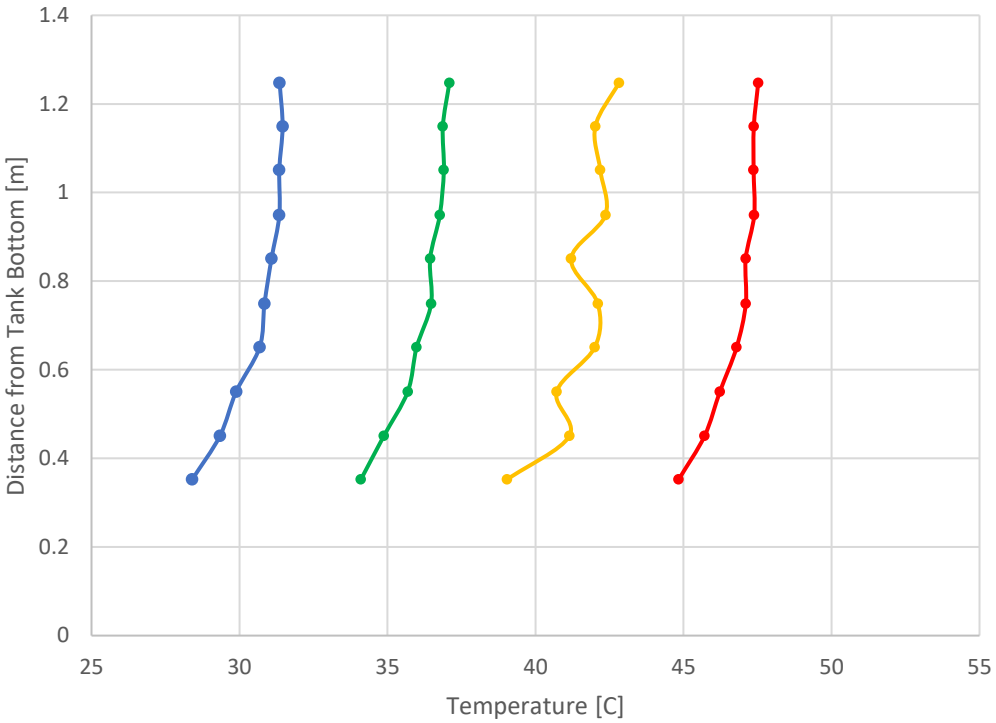

Figure 6.8: Measured water temperatures for system at lower refrigerant charge of 649g.

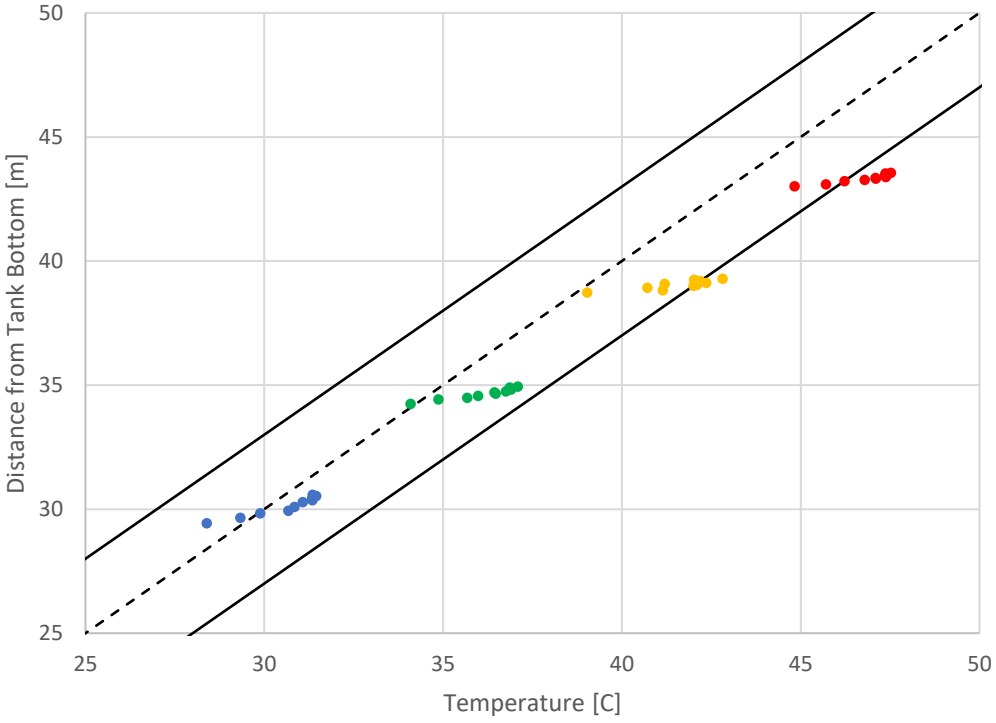

Figure 6.9: Predicted water temperatures (at iteration 2) vs. measured (refrigerant charge = 649g).

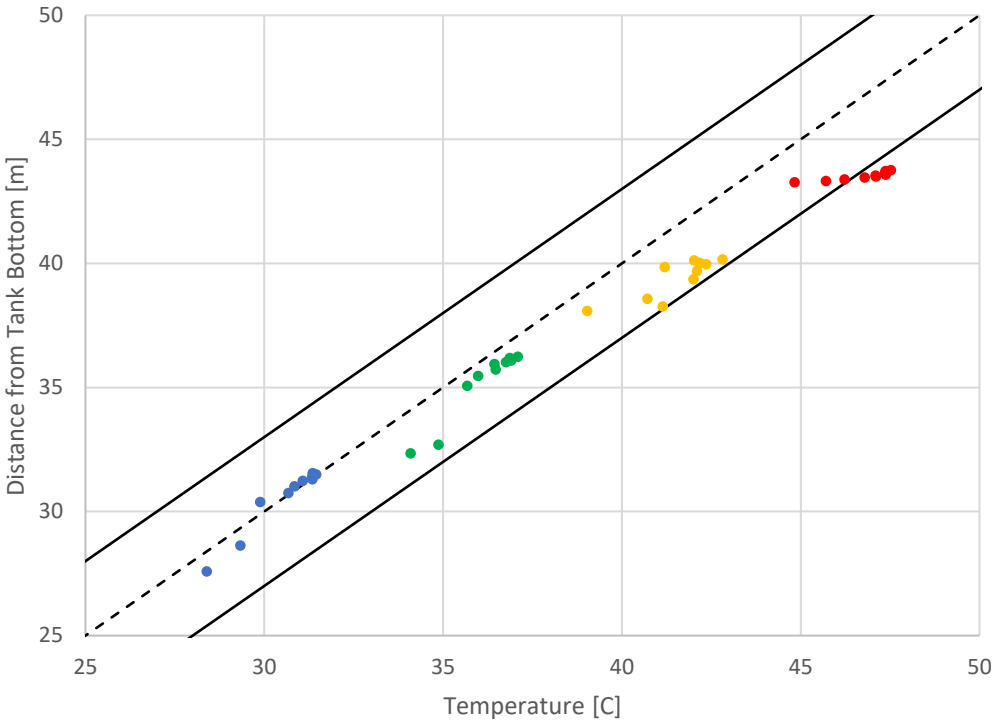

Figure 6.10: Predicted water temperatures (at iteration 5) vs. measured (refrigerant charge = 649g).

CHAPTER 7. ADDITIONAL WORK

7.1 Experimental Response to Varying Refrigerant Charge

A refrigerant charge study was conducted to gain insight into various aspects of HPWH performance and sensitivity over the dynamic and transient nature of the system operation.

From an overall system perspective, refrigerant charge significantly affects warm-up time and efficiency (Figures 7.1 and 7.2). There are also dramatic differences in condenser and water heating performance, exemplified by the thermal stratifications (Figure 7.4) and degrees of subcooling (Figure 7.5).

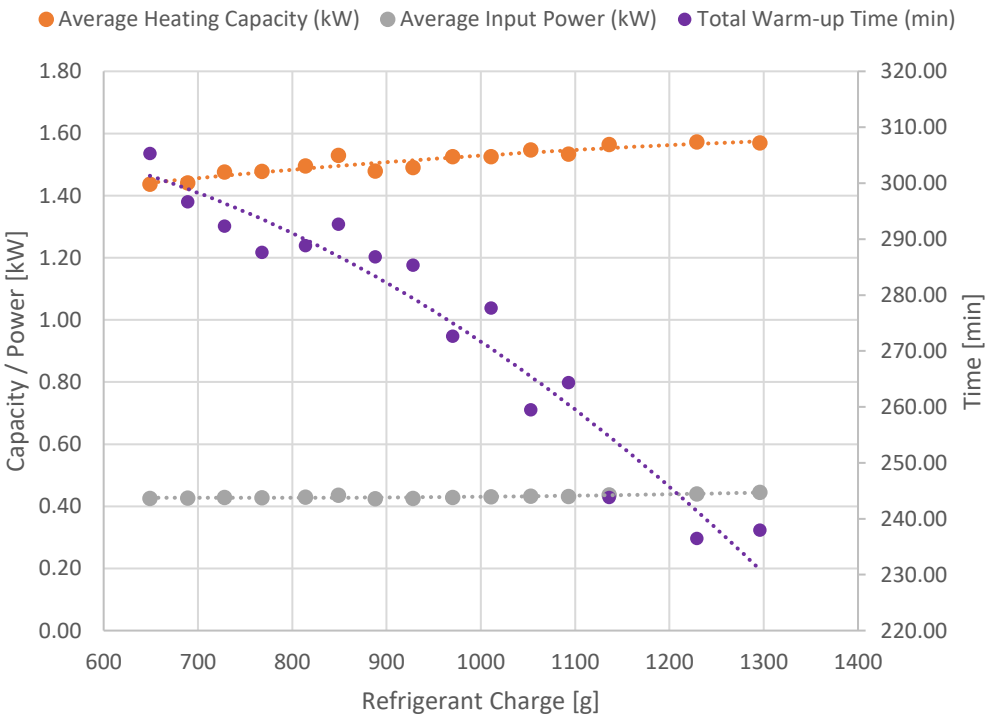

Figure 7.1: Overall heating capacity, input power, and total warm-up times vs. amount of refrigerant charge.

Figure 7.1 shows that as refrigerant charge increases, capacity increases faster than input power at the compressor. Consequently, Figure 7.2 shows an optimal refrigerant charge for COP between 1100-1200g.

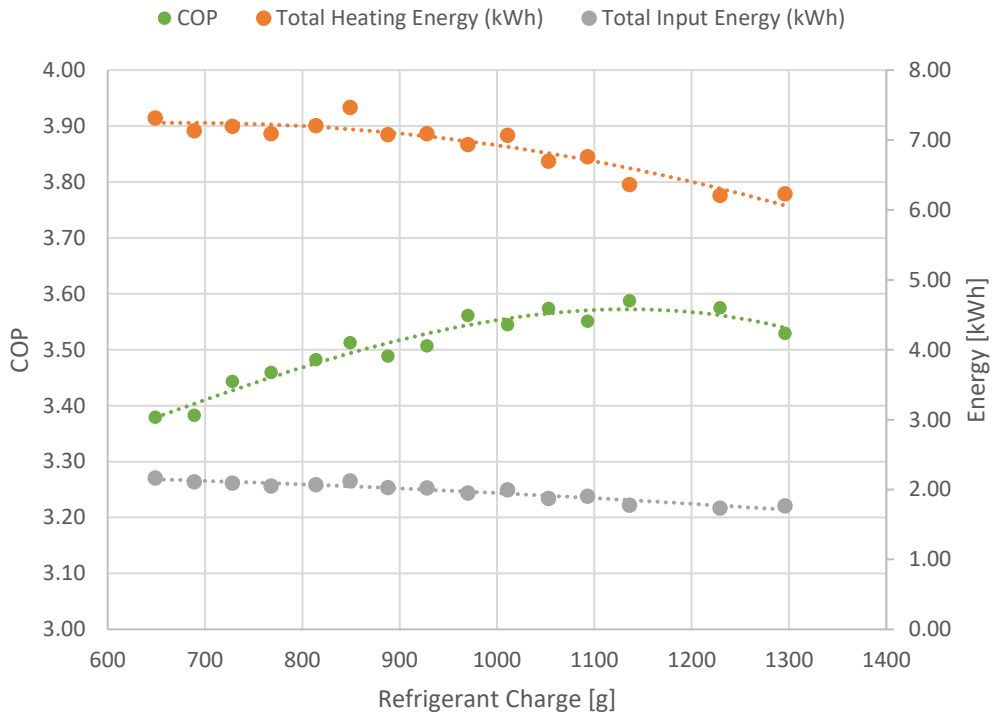

Figure 7.2: COP and total heating and input energy vs. amount of refrigerant charge.

As shown in Figure 7.1 as refrigerant charge increases, heating capacity also increases. This increase in heating capacity allows the system to reach the setpoint water temperature faster. However, from Figure 7.2, it is interesting to note that the total heating energy put to the condenser during the duration decreases even as the capacity increases with additional charge. Figure 7.3 shows the effect of this behavior in terms of final bulk water temperature inside the tank. This bulk temperature is calculated as a volumetric average of temperatures based on their vertical position inside the tank.

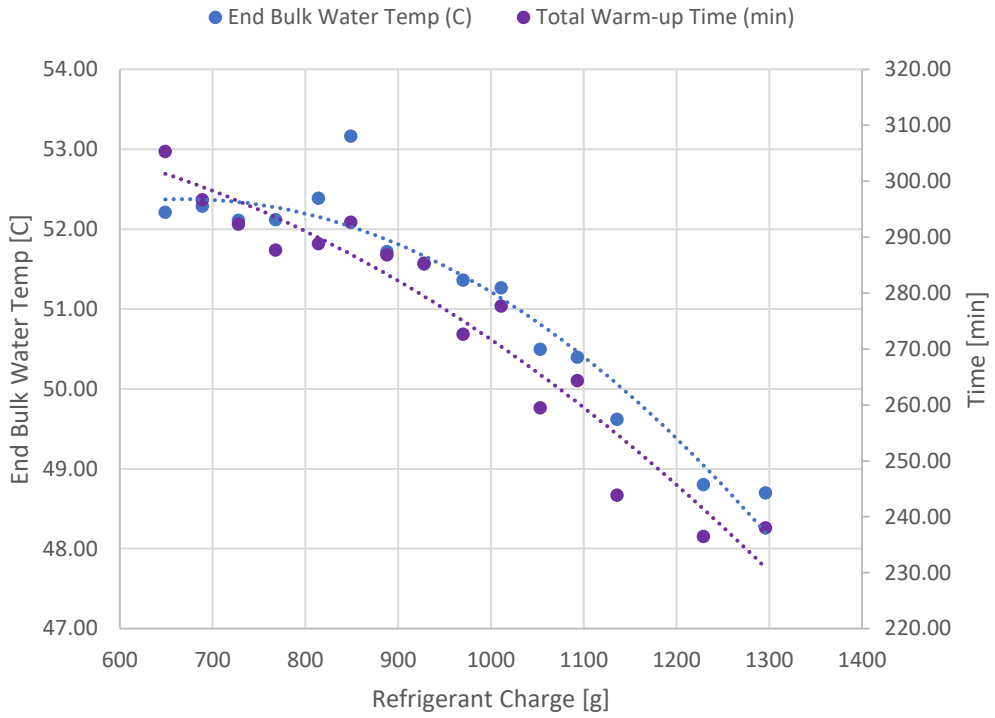

Figure 7.3: End bulk water temperature and warm-up time vs. amount of refrigerant charge.

As shown in Figure 7.3, there is a roughly 5° drop in bulk water temperature over the span of refrigerant charge from low to high. The reason this is possible is due to the increased temperature stratification of the water in the tank as shown in Figure 7.4 caused by the higher heating capacities. In this case, the lowest refrigerant charges exhibited 4-5° of temperature difference between hottest water and the coldest water in the tank while the highest refrigerant charge reached up to 22° of difference. It is also interesting to note that the lower refrigerant charges, with lower heating capacities, tend to have steady or declining stratification over time indicating that the natural mixing inside the tank due to buoyancy effects is effective at mitigating the stratification. On the other hand, operation at the higher charges exhibit a dramatic increase in stratification over time.

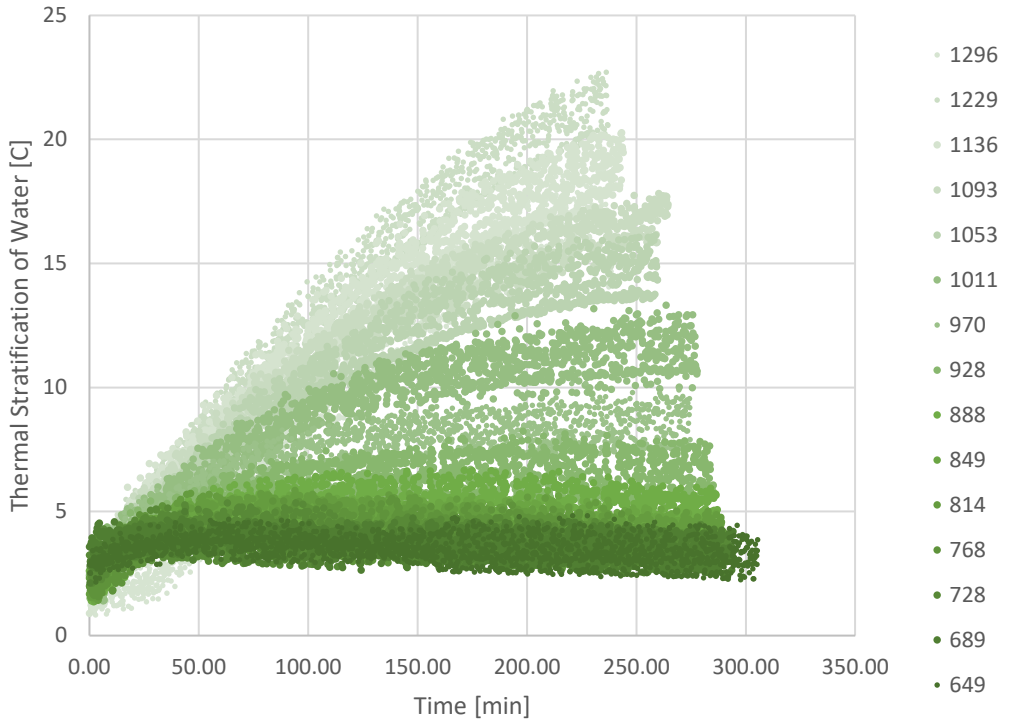

Figure 7.4: Thermal stratification over time for varying amounts of refrigerant charge.

As stated previously, in terms of COP operating efficiency, the optimal charge would lie between 1100-1200g (roughly 300-400g above nominal). Operating at this charge level would also reduce warm-up time to setpoint by 17% or 50min. However, roughly 20° of water temperature stratification would be produced at setpoint, implying that only a fraction of the tank water is viable to supply hot water. Continuing to operate the system at a higher charge, beyond setpoint, would lead to hotter than desired temperatures at the end use. Thus, optimal charge level should also consider actual water demand schedules and the ability of the system to supply enough hot for various demand events through a day. From a design standpoint, it may be prudent to separate the upper and lower coil loops by either putting the loops in parallel or by adding a shut-off for the upper loops allowing the lower loops to bypass and continue heating.

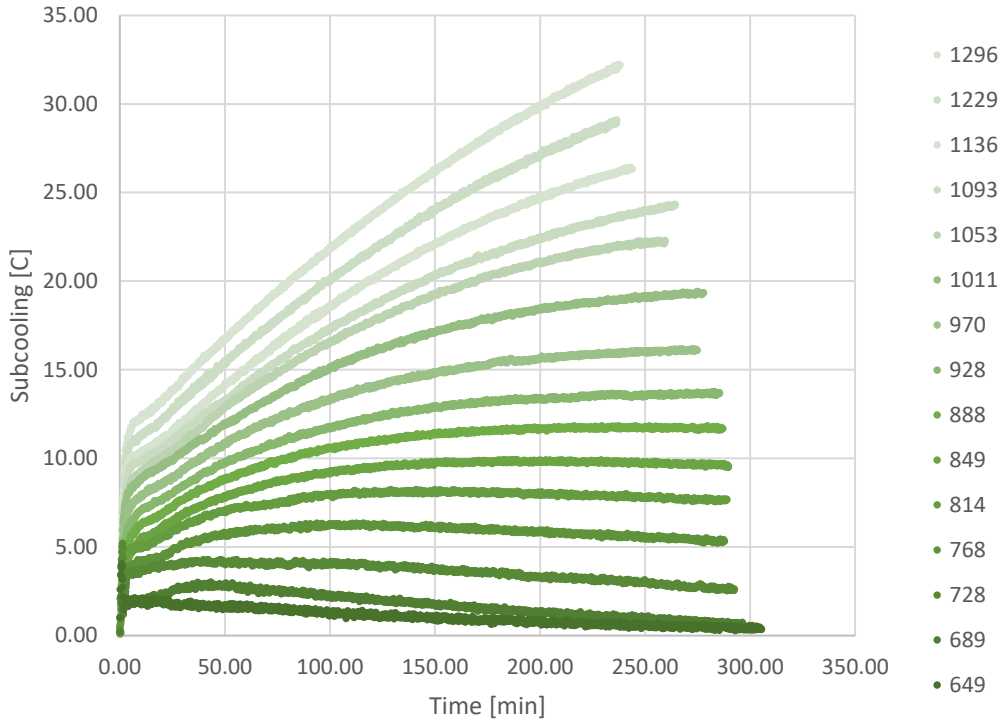

Figure 7.5: Degrees of subcooling over time for varying amounts of refrigerant charge.

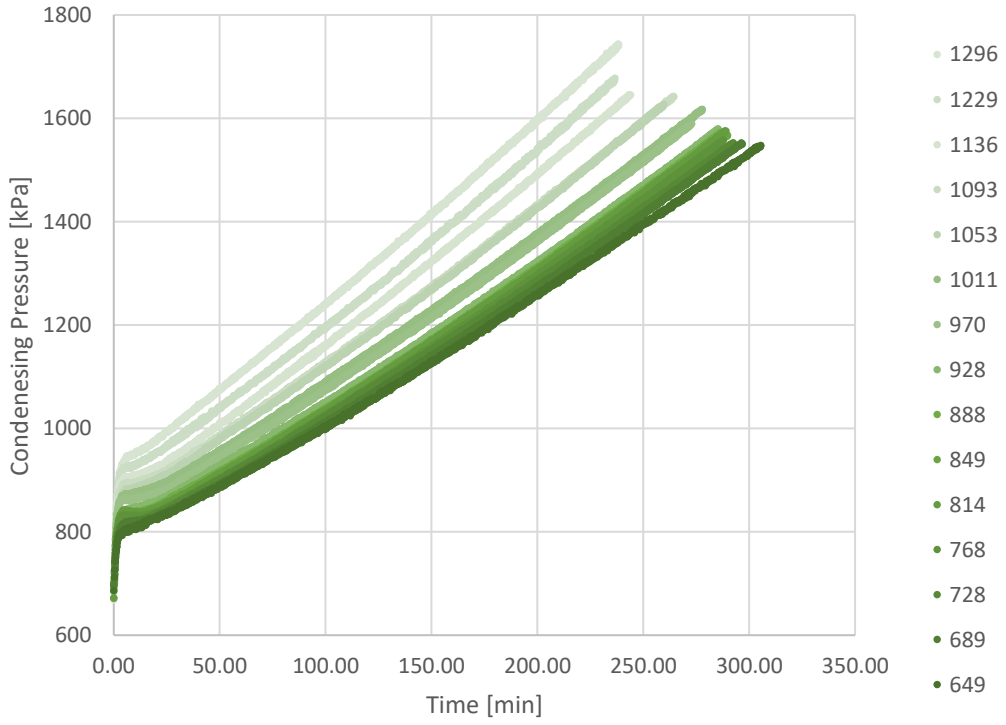

Figure 7.6: Condenser pressure over time for varying amounts of refrigerant charge.

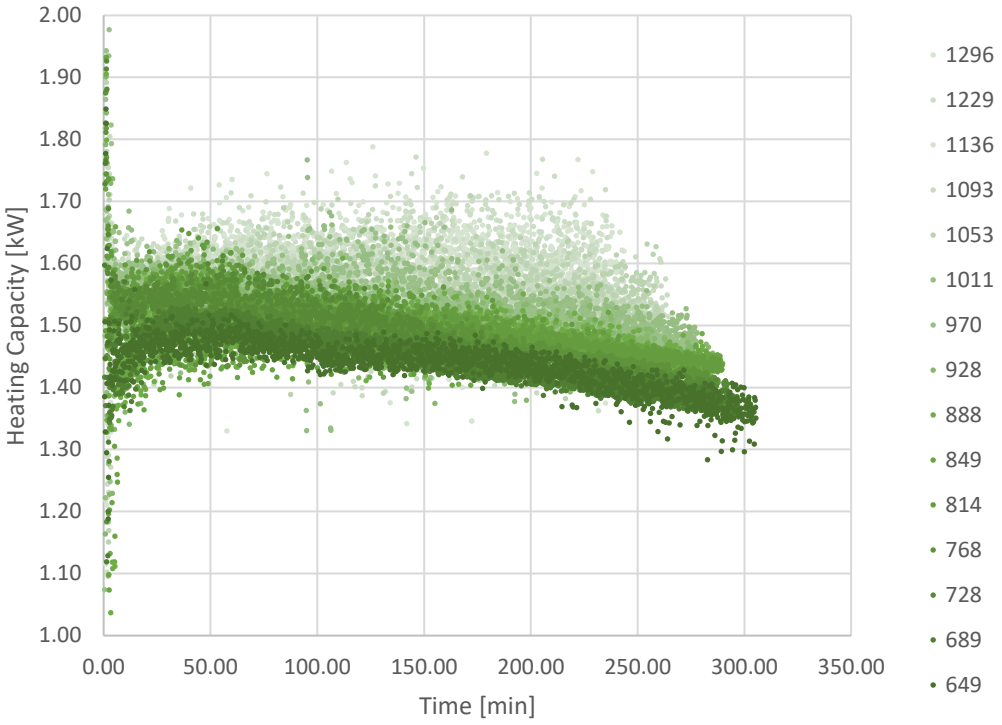

Figure 7.7: Condenser heating capacity over time for varying amounts of refrigerant charge.

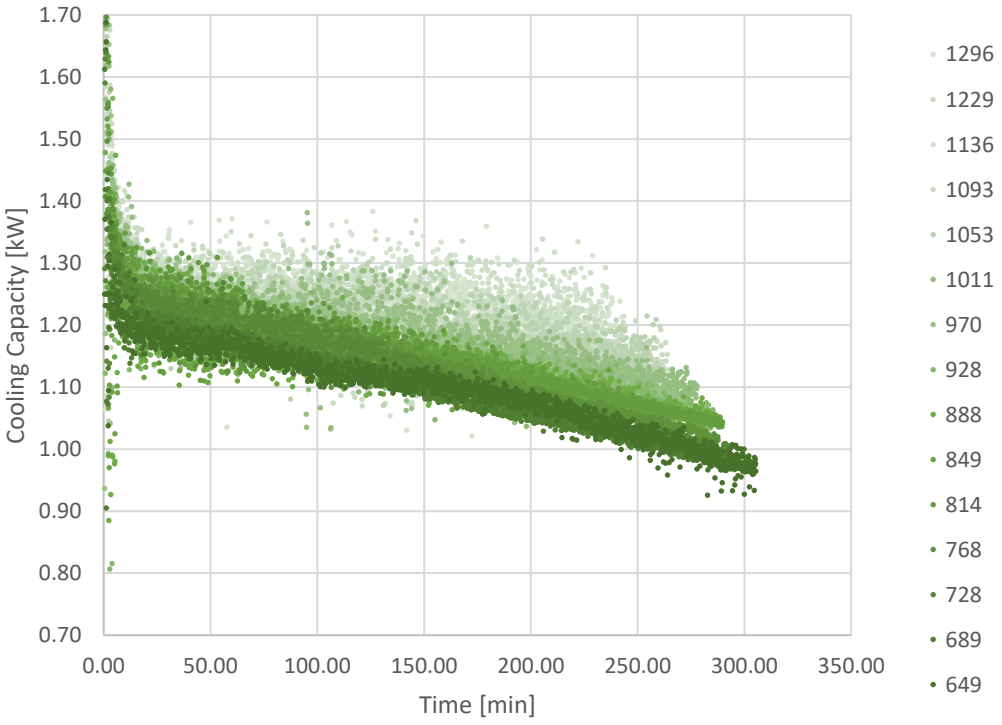

Figure 7.8: Evaporator cooling capacity over time for varying amounts of refrigerant charge.

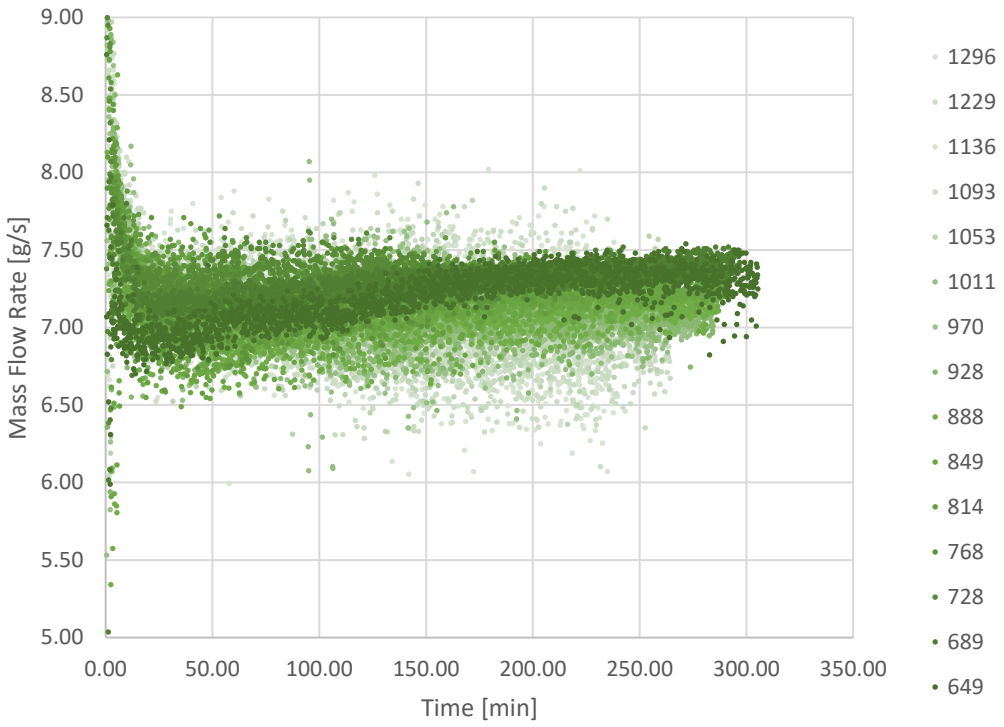

Figure 7.9: Mass flow rate over time for varying amounts of refrigerant charge.

Additional operating characteristics are shown for reference in the charts through Figure 7.9.

7.2 System Performance during High-Temperature Cycling

For heat pump water heaters specifically, another useful mode of operation to evaluate is high-temperature cycling, which would represent shorter draws of hot water (e.g. washing machine cycle, cooled water temperatures after a period of non-use). Clearly, this case exhibits less dynamic behavior, as shown by the property plot shown in Figure 7.10. As a result, for practical purposes, it may be more useful to approximate this specific end use case with a steady-state system model.

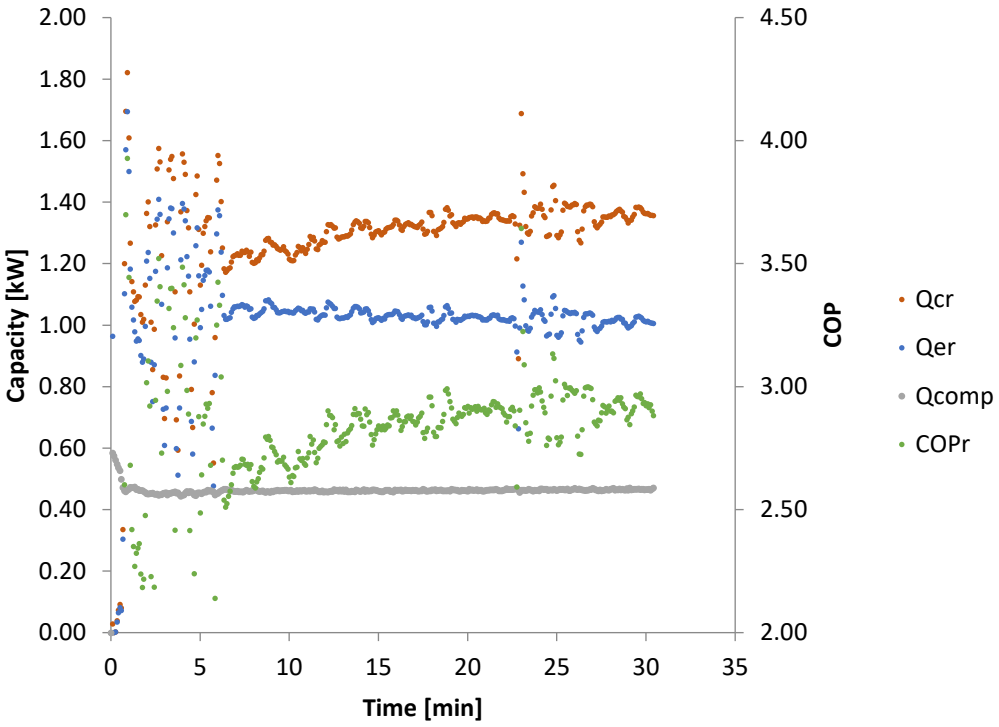

Figure 7.10: System capacity (condenser and evaporator) and efficiency during experimental high-temperature cycling test.

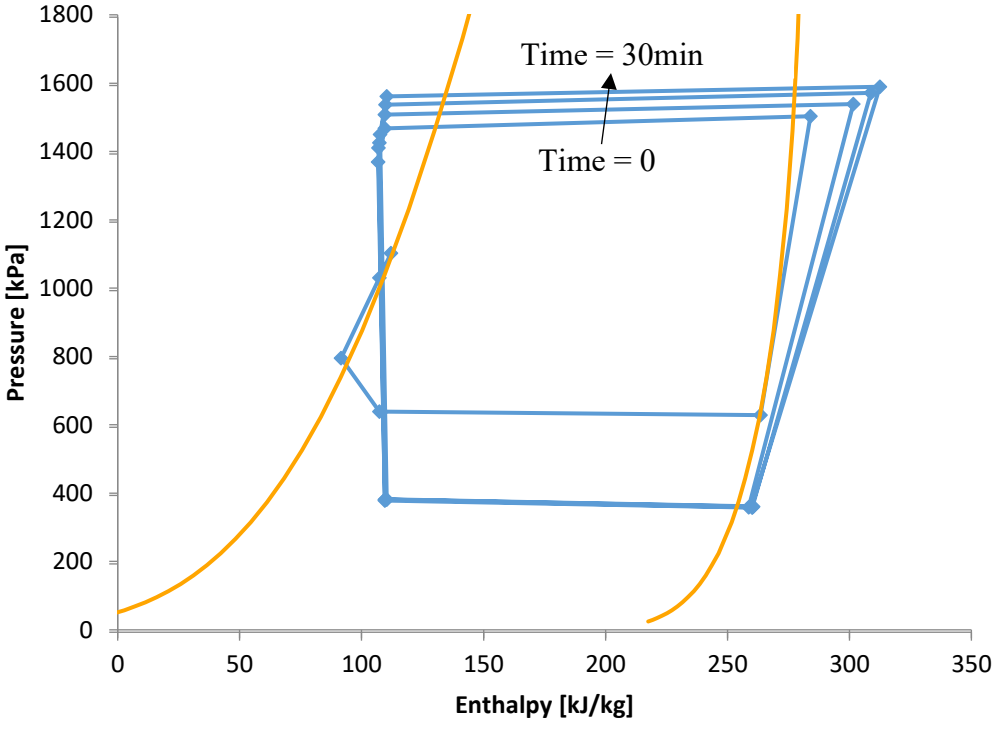

Figure 7.11: High-temperature cycling pressure-enthalpy plot.

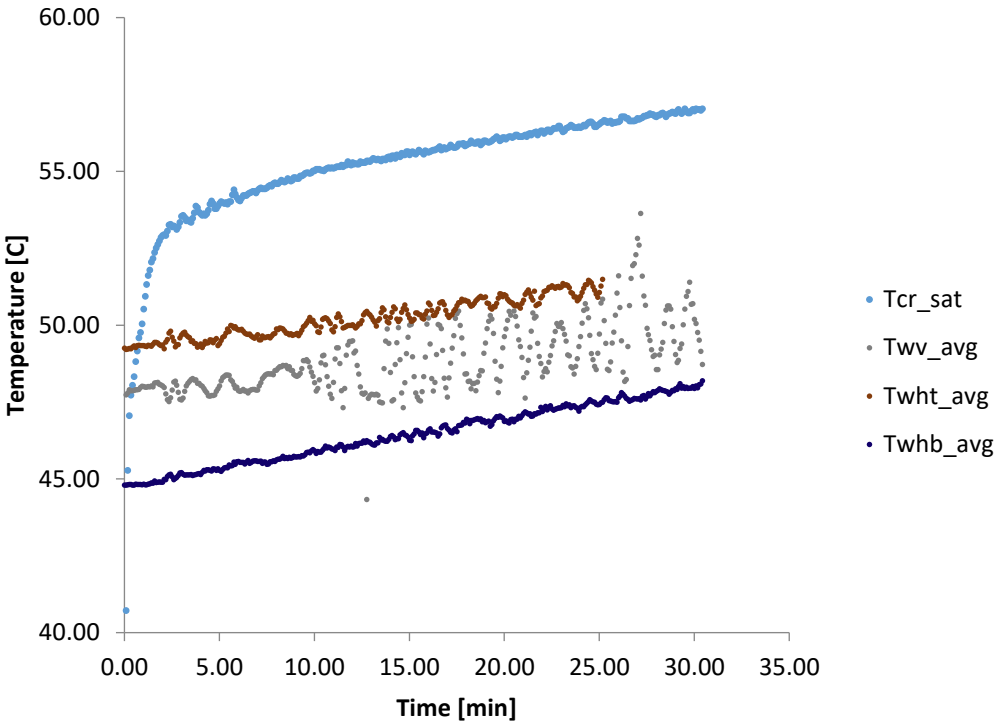

Figure 7.12: High-temperature cycling condenser temperatures.

CHAPTER 8. SUMMARY AND CONCLUSIONS

In this study, a quasi-steady simulation model was developed for a heat pump water heating system that involves the linking of a steady-state vapor compression system model and a transient CFD model of water in the water tank during the heating process.

As seen in the CFD simulation results, temperatures and velocities of the water near the tank wall change during the heating operation and vary from a coil to coil. This dynamic behavior, in turn, affects the spatial heat profile of the system in time, which again alters the fluid dynamics and heating in the water tank. This phenomenon affects the heat transfer rates on a coil by coil basis in the condenser as well as system-level performance. As a result, the linked model was developed to take both phenomena into account.

8.1 RECOMMENDATIONS FOR FUTURE WORK

First, a continuation of linked model iterations would be useful to verify convergence and correlation to the experimental data. In the study above, iterations were concluded at 5.

Second, given the validated model and an accurate depiction of temperature stratification of water in the tank at any given point in time, design

optimizations can be rapidly iterated by evaluating steady-state system models for approximate points in time based on simulated water tank conditions. One would then run a full linked simulation once an optimized design solution set is identified.

Third, the modeling can be further refined by adding a pocket of air at the top of the water tank to simulate real conditions. This could have a small effect on the motion of the water. Additionally, a more precise depiction of contact between the coils and the water tank could be a useful refinement. As stated earlier, in-depth testing over a range of operating conditions to obtain full understanding of contact pressure and thermal conductance for this use case.

Fourth, the CFD model needs a boundary condition added at the cold inlet and hot exit to equalize pressure to city pressure. This would provide a more accurate representation of reality. Unfortunately, this cannot be achieved effectively in the axisymmetric 2D CFD model. This would require a 3D meshed CFD model and significantly more computing resources. However, with a 3D model, water draw can also be taken into account if desired for better approximation of specific end use cases.

Fifth, the simulation experience and utility can be vastly improved by building the system model into the CFD model allowing the system model to run at each time step of the CFD model. This would require rebuilding fluid property look-up tables (built-in to EES) in a format accessible to other scripting languages. In combination with a 3D CFD model, the coil windings could again be represented as a spiral rather than a series of flattened rings.

Finally, as noted in Chapter 3, the temperature data collected by the horizontal thermocouple rods were not particularly insightful. However, this was mainly due to the spacing of the thermocouples in the rod. In hindsight, after viewing the temperature contours outputted by the CFD models, it would be useful to measure the water temperatures close to the tank wall in fine increments. If nothing else, this would be another means of improving the model developed with a better depiction of near-wall behavior.

REFERENCES

Churchill, S. W., "Friction-factor Equation Spans All Fluid Flow Regimes." Chemical Engineering, No. 7, pp.91-92, 1977. Range of correlation: a curve fitting of Moody's friction-factor plots, spanning laminar and turbulent regimes.

Dobson, M.K. and J.C. Chato, 1998, Condensation in Smooth Horizontal Tubes, Journal of Heat Transfer, 120:2, pp.193-213.

Fardoun, Farouk, Oussama Ibrahim, and Assaad Zoughaib. "Quasi-steady state modeling of an air source heat pump water heater." Energy Procedia 6 (2011): 325-330.

Gnielinski, V., "New Equations for Heat and Mass Transfer in Turbulent Pipe and Channel Flow." International Chemical. Engineering., Vol. 16, pp. 359-368, 1976.

Incropera, Frank P., and David P. DeWitt.1990, Fundamentals of Heat and Mass Transfer, New York: Wiley.

Kim, Minsung, Min Soo Kim, and Jae Dong Chung. "Transient thermal behavior of a water heater system driven by a heat pump." International journal of refrigeration 27.4 (2004): 415-421.

Shah, T. and P. Hrnjak. "Linked Modelling of Heat Pump Water Heater Vapor Compression System and Water Tank." 15th International Refrigeration and Air Conditioning Conference at Purdue, West Lafayette, IN, 14-17 July 2014, paper 2431.

Souza, A. L., and Pimenta, M.M., Prediction of pressure drop during horizontal two-phase flow of pure and mixed refrigerants, ASME Conf. Cavitation and multiphase flow, HTD-vol. 210, pp.161-171, 1995.

Zivi, S.M. -1964, Estimation for steady-state steam void fraction by means of the principle of minimum entropy production, Journal of heat transfer, Vol. 86, pp. 247-252.

APPENDIX A: SAMPLE CFD SIMULATION OF NATURAL CONVECTION INSIDE WATER TANK DURING HEATING

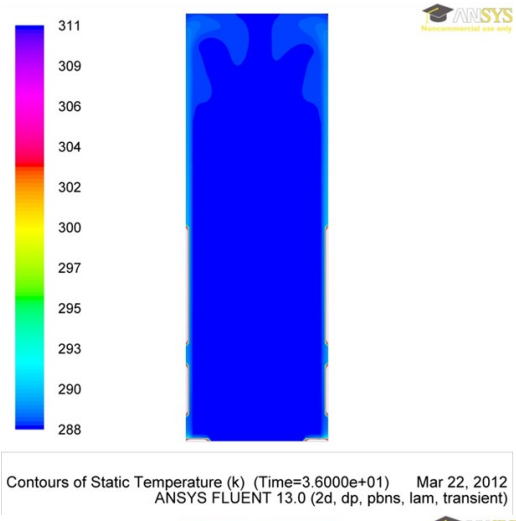

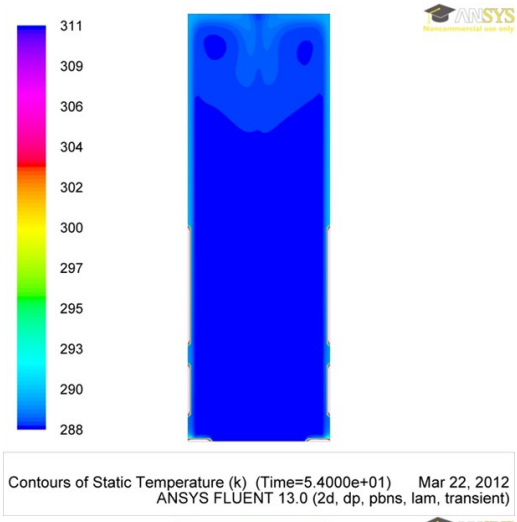

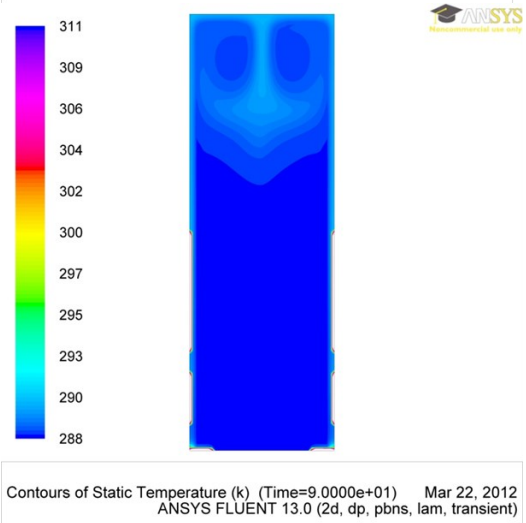

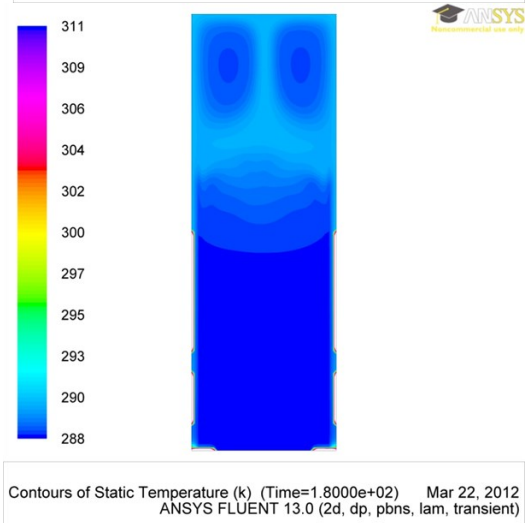

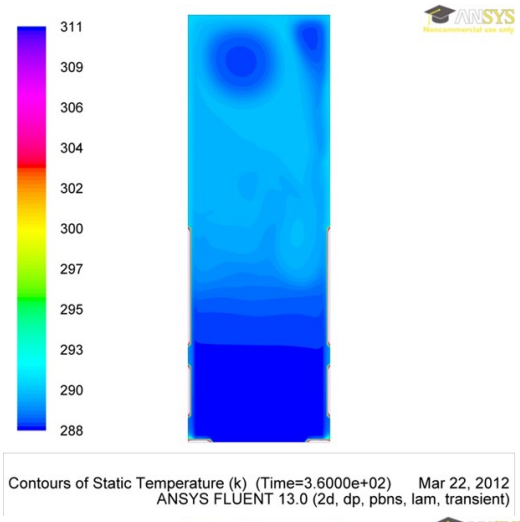

Contours of Static Temperature (k) (Time=3.6000e+02) Mar 22, 2012
ANSYS FLUENT 13.0 (2d, dp, pbns, lam, transient)

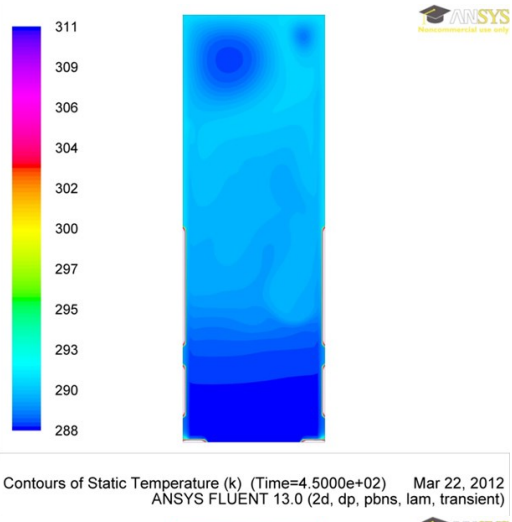

Contours of Static Temperature (k) (Time=4.5000e+02) Mar 22, 2012
ANSYS FLUENT 13.0 (2d, dp, pbns, lam, transient)

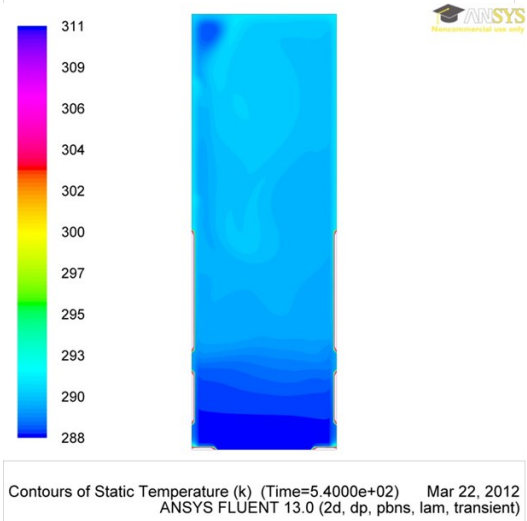

Contours of Static Temperature (k) (Time=5.4000e+02) Mar 22, 2012
ANSYS FLUENT 13.0 (2d, dp, pbns, lam, transient)

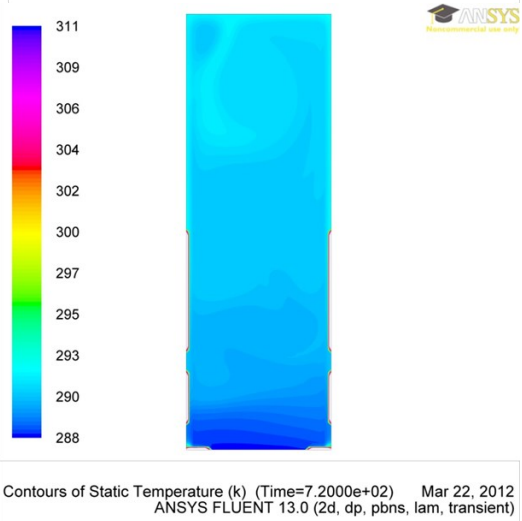

Contours of Static Temperature (k) (Time=7.2000e+02) Mar 22, 2012
ANSYS FLUENT 13.0 (2d, dp, pbns, lam, transient)

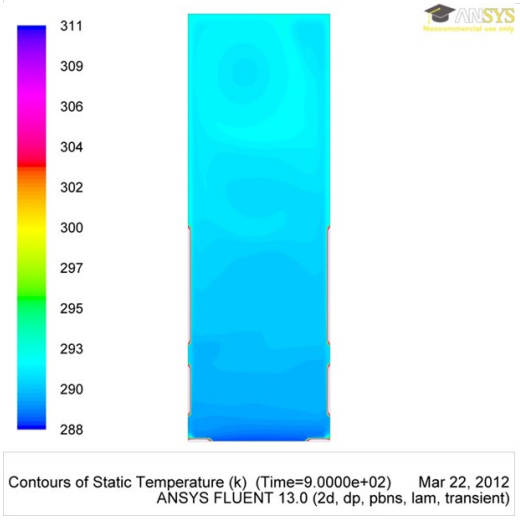

Contours of Static Temperature (k) (Time=9.0000e+02) Mar 22, 2012
ANSYS FLUENT 13.0 (2d, dp, pbns, lam, transient)

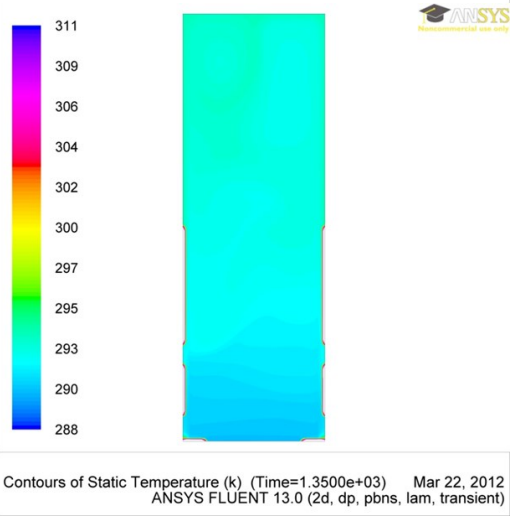

Contours of Static Temperature (k) (Time=1.3500e+03) Mar 22, 2012
ANSYS FLUENT 13.0 (2d, dp, pbns, lam, transient)

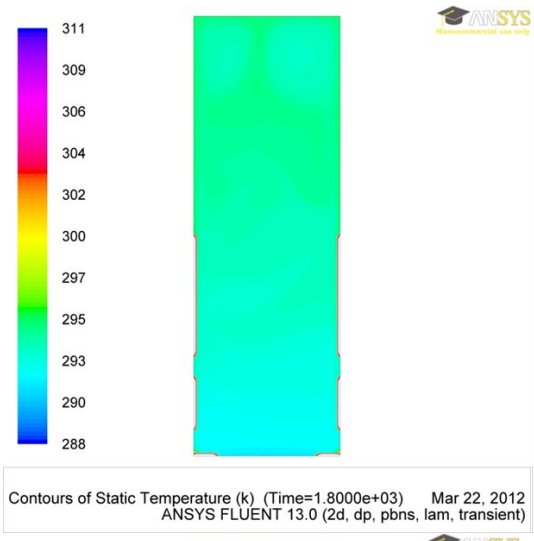
311
309
306
304
302
300
297
295
293
290
288
Contours of Static Temperature (k) (Time=1.8000e+03) Mar 22, 2012
ANSYS FLUENT 13.0 (2d, dp, pbns, lam, transient)

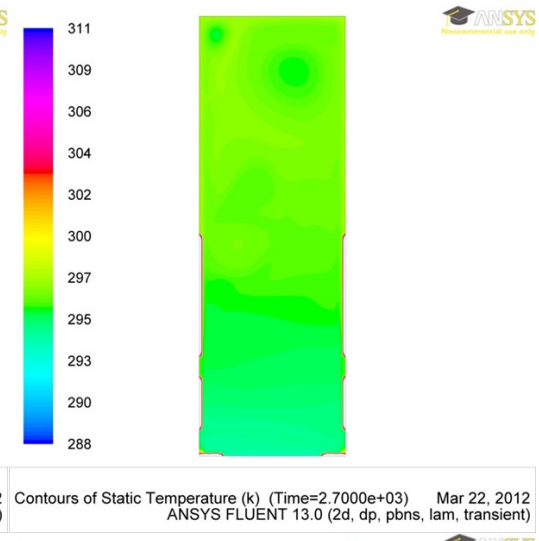
311
309
306
304
302
300
297
295
293
290
288
Contours of Static Temperature (k) (Time=2.7000e+03) Mar 22, 2012
ANSYS FLUENT 13.0 (2d, dp, pbns, lam, transient)

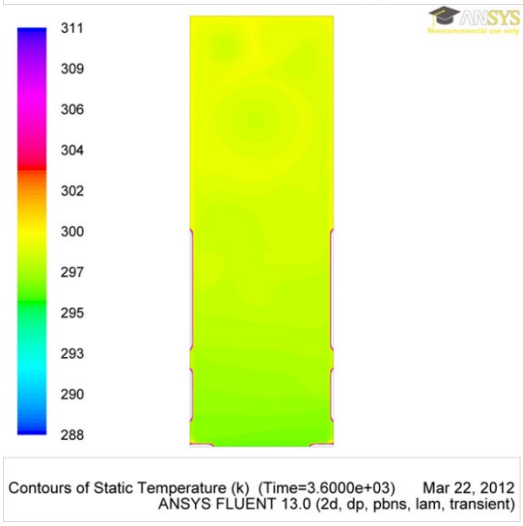
311
309
306
304
302
300
297
295
293
290
288
Contours of Static Temperature (k) (Time=3.6000e+03) Mar 22, 2012
ANSYS FLUENT 13.0 (2d, dp, pbns, lam, transient)

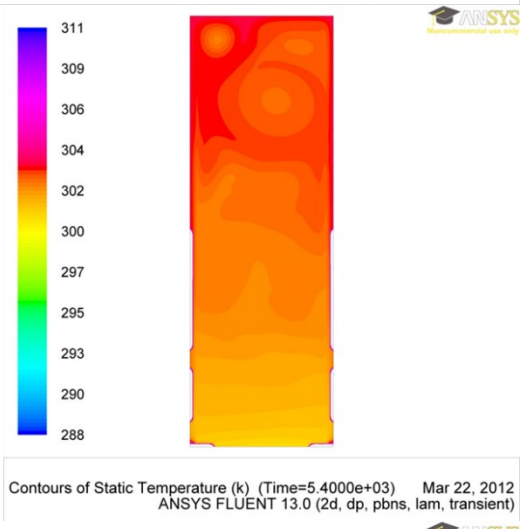
311
309
306
304
302
300
297
295
293
290
288
Contours of Static Temperature (k) (Time=5.4000e+03) Mar 22, 2012
ANSYS FLUENT 13.0 (2d, dp, pbns, lam, transient)

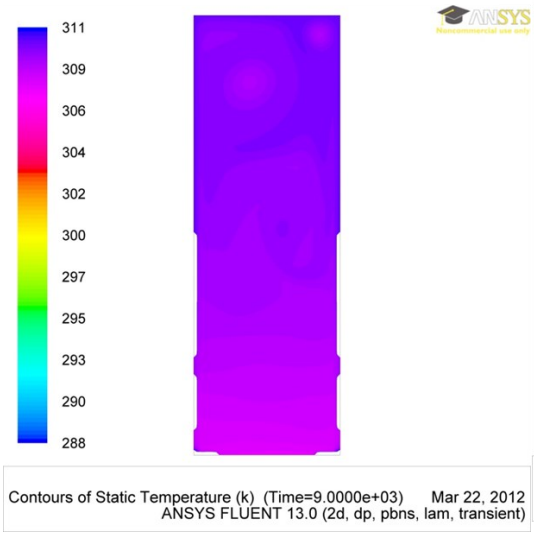
311
309
306
304
302
300
297
295
293
290
288
Contours of Static Temperature (k) (Time=9.0000e+03) Mar 22, 2012
ANSYS FLUENT 13.0 (2d, dp, pbns, lam, transient)

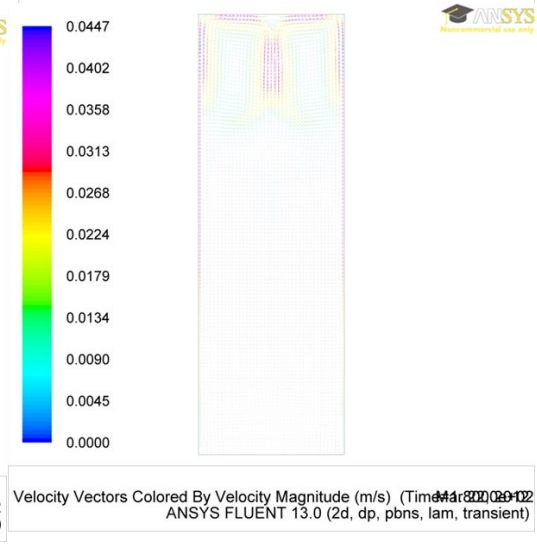
0.0447
0.0402
0.0358
0.0313
0.0268
0.0224
0.0179
0.0134
0.0090
0.0045
0.0000
Velocity Vectors Colored By Velocity Magnitude (m/s)
ANSYS FLUENT 13.0 (2d, dp, pbns, lam, transient)

APPENDIX B: FLUENT CFD UDF CODE (.C)

```
#include "udf.h"

/*Heat Flux Input from EES System Model*/
double ref_time[] = { 0 , 1200 , 3600 , 7200 , 10800 , 14400 , 18000 };
double coil_1[] = { 1.198 , 10.11 , 304.3 , 1081 , 1764 , 2521 , 2916 };
double coil_2[] = { 0.824 , 9.457 , 275.1 , 1115 , 1722 , 2122 , 2185 };
double coil_3[] = { 2.036 , 33.87 , 870.9 , 2142 , 2938 , 3437 , 3161 };
double coil_4[] = { 2.775 , 53.78 , 1298 , 1892 , 2873 , 3461 , 3572 };
double coil_5[] = { 2.015 , 43.12 , 818.8 , 820.6 , 1522 , 1837 , 1773 };
double coil_6[] = { 3.199 , 73.05 , 646.5 , 171.6 , 153.2 , 195.7 , 254.6 };
double coil_7[] = { 9.608 , 209.1 , 981.8 , 452.7 , 523.7 , 624.7 , 699.3 };
double coil_8[] = { 7.518 , 204.9 , 764.1 , 232.8 , 204.9 , 284.2 , 389.7 };
double coil_9[] = { 10.81 , 329.4 , 561.8 , 228.8 , 145.9 , 186.9 , 247 };
double coil_10[] = { 27.12 , 998.9 , 984.9 , 476.8 , 311.6 , 335.5 , 342.2 };
double coil_11[] = { 42.66 , 1377 , 1078 , 593 , 318.7 , 395.9 , 504.5 };
double coil_12[] = { 76.4 , 1561 , 1152 , 942.4 , 358.8 , 315.5 , 226.7 };
double coil_13[] = { 144.6 , 1647 , 1198 , 1026 , 411.3 , 379.6 , 435.4 };
double coil_14[] = { 284.7 , 1735 , 1248 , 1122 , 677.9 , 316.6 , 289.2 };
double coil_15[] = { 576.5 , 1770 , 1262 , 1159 , 757.1 , 415 , 249.7 };
double coil_16[] = { 1211 , 1834 , 1300 , 1207 , 840.1 , 467.8 , 275.7 };
double coil_17[] = { 2385 , 1896 , 1335 , 1229 , 854 , 468.9 , 278 };
double coil_18[] = { 2656 , 1902 , 1337 , 1257 , 877.2 , 461.7 , 255.4 };
double coil_19[] = { 2777 , 1970 , 1378 , 1291 , 899.9 , 456 , 211.2 };
```

```
double coil_20[]        = {  2876  ,  2022  ,  1408  ,
        1304  ,  904.9  ,  446.4  ,  177.6  };
double coil_21[]        = {  2970  ,  2054  ,  1425  ,
        1318  ,  912.5  ,  431.1  ,  142.2  };
double coil_22[]        = {  3046  ,  2091  ,  1448  ,
        1340  ,  914  ,  401.3  ,  105.7  };
double coil_23[]        = {  3135  ,  2132  ,  1473  ,
        1361  ,  919  ,  358.6  ,  74.88  };
double coil_24[]        = {  3214  ,  2174  ,  1501  ,
        1387  ,  921.5  ,  297.4  ,  113.7  };
double coil_25[]        = {  3282  ,  2213  ,  1522  ,
        1391  ,  825.5  ,  261.5  ,  254.1  };
double coil_26[]        = {  3340  ,  2171  ,  1250  ,
        1078  ,  665.9  ,  599.6  ,  621.7  };
double coil_27[]        = {  2522  ,  1686  ,  1472  ,
        1576  ,  1607  ,  1596  ,  1606  };
double coil_28[]        = {  4770  ,  4414  ,  4323  ,
        4580  ,  4592  ,  4488  ,  4405  };

 /*Coil_1*/
 DEFINE_PROFILE(hf_coil_01, t, i)
 {
   face_t f;
   real time = CURRENT_TIME;
          int index;
          int max_index = 6;

          if (time>=3600) {
                  index = (int)(floor(time/3600))+1;
                  if (time >= ref_time[max_index]) {
                          index = max_index - 1;
                  }
          }
          else if (time>=1200) {
                  index = 1;
          }
          else {
                  index = 0;
          }

   begin_f_loop(f,t)
       {
         F_PROFILE(f,t,i) = (coil_1[index+1]-coil_1[index])/(ref_time[index+1]-
ref_time[index])*(time-ref_time[index])+coil_1[index];
       }
   end_f_loop(f,t)
 }

 /*Coil_2*/
 DEFINE_PROFILE(hf_coil_02, t, i)
 {
   face_t f;
   real time = CURRENT_TIME;
          int index;
          int max_index = 6;
```

```
        if (time>=3600) {
                index = (int)(floor(time/3600))+1;
                if (time>=ref_time[max_index]) {
                        index = max_index - 1;
                }
        }
        else if (time>=1200) {
                index = 1;
        }
        else {
                index = 0;
        }

   begin_f_loop(f,t)
       {
         F_PROFILE(f,t,i) = (coil_2[index+1]-coil_2[index])/(ref_time[index+1]-
ref_time[index])*(time-ref_time[index])+coil_2[index];
       }
   end_f_loop(f,t)
 }
```

/*…Code continues for X number for coils */

APPENDIX C: CUSTOM EES FUNCTIONS (.EES)

```
"%%%%%%%%% CFD Profile Functions %%%%%%%%%"

PROCEDURE CFD_PROFILES(tankfluid$, time, use_curvefit_profiles, NUM_coils,
coil_pitch[0..NUM_coils], P_atm : t_UL, velocity_profile[1..NUM_coils],
temp_profile[1..NUM_coils], G_profile[1..NUM_coils], coil_height[1..NUM_coils])
$ARRAYS ON
        time_header$ = String$(time*60) "convert to seconds"

        "Upward Layer Thickness"
        t_UL = 0.02 [m]


        "Curve Fit Coefficients"
        i=1
        repeat
        a[i]=LOOKUP('Water Tank Profiles',i,'Velocity Coeff')
        b[i]=LOOKUP('Water Tank Profiles',i,'Temp Coeff')
        i =i + 1
        until (i>4)


        IF (use_curvefit_profiles>0) THEN
                i = 1
                coil_height[0] = coil_pitch[0]/2
                REPEAT
                        coil_height[i] = coil_height[i-1] + coil_pitch[i-1]/2 + coil_pitch[i]/2

                        "Curve Fitted CFD"
                        {velocity_profile[i] = a[1]*(coil_height[i])^3 + a[2]*(coil_height[i])^2
+ a[3]*(coil_height[i])+a[4]
}
{                       temp_profile[i] = b[1]*(coil_height[i])^3 + b[2]*(coil_height[i])^2 +
b[3]*(coil_height[i])+b[4]
}
                        "CFD Data"
                        velocity_profile[i] = LOOKUP('Velocity CFD Data',i, time_header$)

                        temp_profile[i] = LOOKUP('Temperature CFD Data',i, time_header$) -
273.15

                        i = i+1
                UNTIL(i>NUM_coils)

                ELSE
```

"Velocity Profile"
velocity_profile[1]=SF*0.06
velocity_profile[2]=SF*0.12
velocity_profile[3]=SF*0.03
velocity_profile[4]=SF*0.03
velocity_profile[5]=SF*0.10
velocity_profile[6]=SF*0.10
velocity_profile[7]=SF*0.04
velocity_profile[8]=SF*0.08
velocity_profile[9]=SF*0.08
velocity_profile[10]=SF*0.03
velocity_profile[11]=SF*0.03
velocity_profile[12]=SF*0.03
velocity_profile[13]=SF*0.03
velocity_profile[14]=SF*0.03
velocity_profile[15]=SF*0.03
velocity_profile[16]=SF*0.03
velocity_profile[17]=SF*0.03
velocity_profile[18]=SF*0.03
velocity_profile[19]=SF*0.03
velocity_profile[20]=SF*0.03
velocity_profile[21]=SF*0.03
velocity_profile[22]=SF*0.03
velocity_profile[23]=SF*0.03
velocity_profile[24]=SF*0.03
velocity_profile[25]=SF*0.03
velocity_profile[26]=SF*0.03
velocity_profile[27]=SF*0.03
velocity_profile[28]=SF*0.03

"Temperature Profile"
temp_profile[1]=SF*0.06
temp_profile[2]=SF*0.12
temp_profile[3]=SF*0.03
temp_profile[4]=SF*0.03
temp_profile[5]=SF*0.10
temp_profile[6]=SF*0.10
temp_profile[7]=SF*0.04
temp_profile[8]=SF*0.08
temp_profile[9]=SF*0.08
temp_profile[10]=SF*0.03
temp_profile[11]=SF*0.03
temp_profile[12]=SF*0.03
temp_profile[13]=SF*0.03
temp_profile[14]=SF*0.03
temp_profile[15]=SF*0.03
temp_profile[16]=SF*0.03
temp_profile[17]=SF*0.03
temp_profile[18]=SF*0.03
temp_profile[19]=SF*0.03
temp_profile[20]=SF*0.03
temp_profile[21]=SF*0.03
temp_profile[22]=SF*0.03
temp_profile[23]=SF*0.03
temp_profile[24]=SF*0.03
temp_profile[25]=SF*0.03

```
temp_profile[26]=SF*0.03
temp_profile[27]=SF*0.03
temp_profile[28]=SF*0.03
        ENDIF

        j = 1
        REPEAT
                rho[j]=Density(tankfluid$,T=temp_profile[j],P=P_atm)
                G_profile[j] = rho[j]*velocity_profile[j]
                j = j + 1
        UNTIL (j>NUM_coils)
END


PROCEDURE Natural_Convection_Vertical(tankfluid$, v_fluid,T_fluid, P_fluid, L : h_natural)
"       Nusselt = external flow over flat plate, laminar, average
"



{       IF (T_fluid>T_surface) THEN
                REPEAT
                        T_surface = T_fluid + 0.1
                UNTIL (T_surface>T_fluid)
        ENDIF}

        g = 9.81
        beta = VolExpCoef(tankfluid$,T=T_fluid,P=P_fluid)
        rho = Density(tankfluid$,T=T_fluid,P=P_fluid)
        Pr = Prandtl(tankfluid$,T=T_fluid,P=P_fluid)
        cp = Cp(tankfluid$,T=T_fluid,P=P_fluid)
        k = Conductivity(tankfluid$,T=T_fluid,P=P_fluid)
        alpha = k/(rho*cp)
        mu = Viscosity(tankfluid$,T=T_fluid,P=P_fluid)

        Re = rho*v_fluid*L/(mu)

        Nusselt = 0.664*Re^(1/2)*Pr^(1/3)
        h_natural = Nusselt*k/L*CONVERT(W,kW)

END

PROCEDURE  Prop_Fluid(fluid$,Ta, P:cp_air, mu_air, rho_air, Pr_air)
        cp_air=SPECHEAT(fluid$,T=Ta,P=P)                "Specific heat, [kJ/kg-K]"
        mu_air=VISCOSITY(fluid$,T=Ta,P=P)               "Viscosity, [kg/m-s]"
        rho_air=DENSITY(fluid$,T=Ta,P=P)            "Density  [kg/m^3]"
        Pr_air=PRANDTL(fluid$,T=Ta,P=P)                 " Prandtl number "
END

PROCEDURE Metal_Contact(metal_1$,metal_2$, P_contact,R_contact_perarea_default :
R_contact_perarea)
        R_contact_perarea = R_contact_perarea_default
        IF (CONCAT$(metal_1$,metal_2$)='CopperStainless_AISI304') OR
(CONCAT$(metal_1$,metal_2$)='Stainless_AISI304Copper') THEN
                R_contact_perarea=1/15.175
                IF (P_contact=100) THEN
                        R_contact_perarea=1/15.500
```

```
                ENDIF
        ENDIF
END

PROCEDURE Metal_Cond(metal_$,T_high,T_low : k_fin)
        k_fin=k_(metal_$, AVERAGE(T_high,T_low))
END

PROCEDURE ElementCal_Wraparound(tankfluid$,D_tank,h_tank,t_insulation,t_tank,
L_contact,D_inner,D_outer,coil_num,NUM_coils,NUM_elements_percoil,coil_pitch[0..NUM_co
ils],m_dot_r : DL,A_fin_r,A_fin_w,A_contact,G_r,Vol)

        DL=SQRT((PI*(D_tank+D_outer+2*t_tank))^2+(coil_pitch[coil_num])^2)/NUM_eleme
nts_percoil
        A_fin_r=2*PI*(D_outer/2)*DL

        N=5
        N=NUM_coils
        Sum=0
        i=0
        REPEAT
                Sum = Sum+coil_pitch[i]
                i=i+1
        UNTIL (i>NUM_coils)


{       coil_pitch[NUM_coils+1]=h_tank-SUM(coil_pitch[i],i=0,N)}

        IF (coil_num<>1) AND (coil_num<>NUM_coils) THEN
                A_fin_w=2*(coil_pitch[coil_num]/2)*DL
                ELSE
                        IF (coil_num=1) THEN
                                A_fin_w=2*((coil_pitch[1]+coil_pitch[0])/2)*DL
                        ENDIF
                        IF (coil_num=NUM_coils) THEN
                                A_fin_w=2*((coil_pitch[NUM_coils]{+(h_tank-
Sum)})/2)*DL
                        ENDIF
        ENDIF

        A_contact=L_contact*DL
        A_r_xc=(PI*(D_inner)^2)/4
        G_r=m_dot_r/A_r_xc
        Vol=A_r_xc*DL

END

PROCEDURE Eff_rectfin(htc_fluid,k_fin,t_fin,height_fin : Eff_fin)
"       htc_fluid = [kW/K]
        k_fin = [W/m-K]
"
        mL=(2*htc_fluid/((k_fin*CONVERT(W,kW))*t_fin))^0.5*height_fin
        Eff_Fin=tanh(mL)/(mL)

END
```

```
PROCEDURE UA_HPWH(Eff_fin_r, h_r, A_fin_r, Eff_fin_w, h_w, A_fin_w,
R_contact_perarea, A_contact :UA,U, R_r, R_w, R_contact)

        R_r=(Eff_fin_r*h_r*A_fin_r)^(-1)
        R_w=(Eff_fin_w*h_w*A_fin_w)^(-1)
        R_contact=R_contact_perarea/A_contact

        UA=1/(R_r+R_w+R_contact)
        U=UA/A_fin_w

END
```